Fragility functions for tall URM buildings around early 20th century in Lisbon. Part 1: methodology and application at building level

Ana G. Simões[1], Rita Bento[1*], Sergio Lagomarsino[2], Serena Cattari[2], Paulo B. Lourenço[3]
[1]CERIS, Instituto Superior Técnico, Universidade de Lisboa, Lisbon (Portugal)
[2]DICCA, Università Degli Studi di Genova, Genoa (Italy)
[3]ISISE, Universidade do Minho, Campus de Azurém, Guimarães (Portugal)
*Corresponding Author: Address: Av. Rovisco Pais, 1, 1049-001 Lisboa, Portugal;
Email: rita.bento@tecnico.ulisboa.pt; Tel: +351 218 418 210

Abstract
The article proposes a procedure for the derivation of fragility functions for unreinforced masonry buildings considering the in-plane and out-of-plane response. Different approaches are considered for the generation of the corresponding fragility functions and for the evaluation of the propagation of uncertainties. The contributions for the dispersion of the fragility functions account for the variability in the definition of the capacity, the aleatory uncertainty in the definition of the seismic demand and the aleatory uncertainty in the definition of the modified/floor response spectrum, when the local mechanisms are located in the upper level of the building. In the end, the individual fragility curves are properly combined in order to define a single fragility curve for the class of buildings. As a case study, the procedure is applied to the assessment of one of the most vulnerable unreinforced masonry buildings constructed in the early 20th century in Lisbon, considering a typical prototype building with five storeys high. Results for a seismic event, as defined in the earthquake-resistant code for Lisbon, indicate that the typical building has about 50% probability of having heavy damage and about 30% probability of collapse.

Keywords
Unreinforced Masonry Buildings; Seismic Vulnerability; Fragility Functions; Non-Linear Static Analysis; Non-Linear Kinematic Analysis; Performance-Based Assessment

1. Introduction

It is known that, in case of an earthquake, the victims and economic losses are mainly related to the seismic behaviour of structures. Previous studies regarding seismic risk analysis in mainland Portugal indicated that masonry buildings are the most seismically vulnerable and also the most common building typology (Silva et al. 2015). Lisbon area has the highest seismic hazard in Portugal and particular attention should be given to the residential unreinforced masonry (URM) buildings constructed in the transition between the 19th and 20th centuries. These buildings characterize a period of low construction quality in Lisbon with relatively tall buildings (between four and six storeys), particularly in comparison with the preceding earthquake-resistant masonry buildings constructed after the 1755 earthquake (Simões et al. 2015). They are commonly referred to as "gaioleiro" buildings, meaning "bird cage", as they seem more adequate for birds than people (Appleton, 2005; Simões et al., 2017). The main objective of this work is to present a procedure for the derivation of fragility functions and to evaluate the seismic vulnerability of such tall URM buildings in Lisbon.

Seismic vulnerability addresses the susceptibility to suffer damage or loss due to an earthquake. It can be defined using fragility functions, providing the probability of reaching or exceeding a specified limit state as a function of the intensity of a seismic event, or using vulnerability functions, providing the expected value of loss. There are several methods available for the derivation of fragility functions, classified into four categories (Porter et al. 2007; Pitilakis, 2014): empirical, expert elicitation/judgement, analytical and hybrid. Erberik (2008) proposed fragility functions for masonry typologies in Turkey, taking into account structural variations within each building typology (e.g. number of stories, load-bearing wall material, regularity in plan and arrangement of walls). The buildings capacity curves were obtained through non-linear static (pushover) analyses. Rota et al. (2010) proposed fragility functions for masonry buildings based on the convolution between the probability density function of a specific limit state, determined based on non-linear static (pushover) analyses, and the probability distribution of the seismic demand, obtained from non-linear dynamic time-history analyses. In both cases, the mechanical properties of masonry were analysed as aleatory variables and only the in-plane response of the buildings was considered.

This article proposes a procedure to derive fragility functions for URM buildings based on non-linear analyses but considering the in-plane and out-of-plane response of the buildings and the propagation of uncertainties (Figure 1). The in-plane response refers to the global (box-type) behaviour controlled by the in-plane capacity of walls and stiffness of floors. The out-of-plane response refers to the activation of local mechanisms, typically consisting on the overturning of parts of the building insufficiently connected to the rest of the structure. The capacity curves are obtained, for the in-plane response, through non-linear static (pushover) analyses, and, for the out-of-plane response, through non-linear kinematic analyses. The aleatory variables associated with the analyses are, respectively, treated by the Monte Carlo Method (Rubinstein, 2011) and by the Response Surface Technique (Liel et al. 2009; Ottonelli, 2015). The limit states (LS) are defined according to the criteria proposed by Cattari and Lagomarsino (2013a) that correlates the behaviour of the structure at three scales: element, macro-element and global. A new formulation for the macro-element scale is applied to detect the activation of soft storey mechanisms (Marino et al.; 2018). The intensity measure (IM) that produces the attainment of the limit state is obtained from the application of the Capacity-Spectrum Method with overdamped spectrum and without any iterative procedure, as proposed in (Lagomarsino et al., 2015). The final dispersion of the fragility curves results from the contribution of the dispersion in the capacity and the dispersion in the seismic demand. The approach adopted for the derivation of fragility functions is described in detail in the following sections. The procedure is after applied to the determination of the seismic vulnerability of a typical class of URM "gaioleiro" buildings. In a companion article (Simões et al., 2019a) the procedure is applied to different classes of buildings aiming at the overall assessment of the seismic vulnerability of this class of buildings in Lisbon.

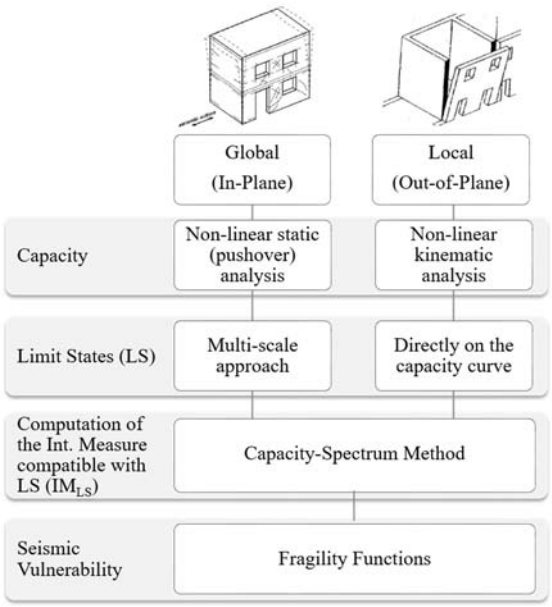

Figure 1 – Procedure for the definition of fragility functions for URM buildings

2. Approach adopted for the derivation of fragility functions

Fragility functions provide the probability of reaching or exceeding a certain limit state (LS) as a function of a selected seismic intensity measure (IM). The seismic behaviour of URM buildings is usually divided between in-plane and out-of-plane response. The common approach is to neglect the mutual interaction between these responses and to analyse them independently. Accordingly, to such approach, in this work, the fragility functions are firstly obtained numerically, based on non-linear analysis and detailed models, for both the global and local behaviour, and then they are combined to define a single final fragility curve.
Fragility functions are herein described by a lognormal cumulative distribution function, as:

$$p_{LS}(im) = P(d \geq D_{LS} \mid im) = P(im_{LS} < im) = \Phi\left(\frac{1}{\beta_{LS}} \log\left(\frac{im}{IM_{LS}}\right)\right) \quad (1)$$

where: d is a displacement representative of the seismic behaviour, D_{LS} is the displacement limit state threshold, Φ is the standard cumulative distribution function, IM_{LS} is the median value of the lognormal distribution of the intensity measure that produces the attainment of the limit state threshold LS, and β_{LS} is the dispersion.
Among other possible choices (Douglas et al. 2015), the intensity measure adopted is the peak ground acceleration (PGA), which is a common choice in case of URM buildings. This option, despite being unable to represent the full contents of the seismic signal, is also quite effective for a direct interpretation of results and for the comparison with other studies available in the literature.
The intensity measure compatible with LS, IM_{LS}, is obtained from the application of the Capacity-Spectrum Method with overdamped spectrum and without any iterative procedure, as proposed in (Lagomarsino et al., 2015). The procedure is based on the comparison between the displacement capacity of the structure for a limit state threshold (D_{LS}) and the seismic demand, in an acceleration-displacement coordinates system. The displacement capacity of the structure is defined on its capacity curve, which gives the acceleration of an equivalent non-linear single-degree-of-freedom (SDOF) system as a function of its displacement. The seismic demand is expressed by an acceleration-displacement response spectrum (ADRS), which gives the spectral acceleration S_a as a function of the spectral displacement S_d, for an equivalent viscous damping $\xi=\xi_{el}=5\%$, considered valid in the initial elastic range. Finally, the intensity measure IM_{LS} is determined from:

$$IM_{LS} = \frac{D_{LS}}{S_{d1}(T_{LS})\eta(\xi_{LS})} \quad (2)$$

where: S_{d1} is the displacement response spectrum, T_{LS} is the linear equivalent period corresponding to the limit state threshold, defined by Equation (3) and, $\eta(\xi_{LS})$ is the damping correction factor, defined by Equation (4).

$$T_{LS} = 2\pi\sqrt{\frac{D_{LS}}{A(D_{LS})}} \quad (3)$$

$$\eta(\xi_{LS}) = \sqrt{\frac{10}{5+\xi_{LS}}} \tag{4}$$

The overdamped spectrum is obtained by multiplying the normalized response spectrum by $\eta(\xi_{LS})$. The equivalent viscous damping (ξ_{LS}) takes into account the contribution of the initial elastic viscous damping (ξ_{el}) and the hysteretic damping ($\xi_{h,LS}$), as defined by:

$$\xi_{LS} = \xi_0 + \xi_{h,LS} \tag{5}$$

The dispersion of the fragility curve (β_{LS}) takes into account two different contributions: 1) the aleatory variability in the definition of the capacity (β_C) and, 2) the aleatory uncertainty in the definition of the seismic demand (β_D). Other contributions may be considered (Lagomarsino, 2014). Under the hypothesis that these contributions are statistically independent, dispersion β_{LS} reads:

$$\beta_{LS} = \sqrt{\beta_C^2 + \beta_D^2} \tag{6}$$

The variability in the definition of the capacity (β_C) is related to random/aleatory variables. These aim to account for the uncertainties in the quantification of specific parameters and the intrinsic variations between buildings. Different parameters are assumed as aleatory variables for the analysis of the global and local behaviour and then included in the evaluation of the propagation of uncertainties. The aleatory uncertainty in the definition of the seismic demand (β_D) is related to the variability of the seismic input described by the intensity measure, as:

$$\beta_D = 0.5\left|\log(IM_{LS,84}) - \log(IM_{LS,16})\right| \tag{7}$$

where $IM_{LS,84}$ and $IM_{LS,16}$ are the IM_{LS} values that produce the attainment of the limit state threshold LS by considering as input the 84% and 16% percentiles ($S_{a,16}$ and $S_{a,84}$, respectively) of the elastic response spectrum. The IM_{LS} values are determined by considering the median capacity curve, whereas the referred response spectra are determined starting from a selection of a set of real ground-motion records compatible with the geophysical characteristics of the reference code seismic action.

Figure 2 plots the response spectra corresponding to these 84% and 16% percentiles and compares the response spectrum corresponding to the 50% percentile ($S_{a,50}$) with the code response spectrum ($S_{a,Code}$) defined for Lisbon according to Part 1 of Eurocode 8, EC8-1 (IPQ, 2010). In particular, the latter has been obtained by assuming seismic action type 1 (intra-plate earthquake), zone 3 (PGA=1.50 m/s^2) and soil type B (S=1.29). The real ground-motion records were selected with SelEQ tool (Macedo and Castro 2017), a software application that features a wide variety of filtering criteria. A total of 30 records was considered.

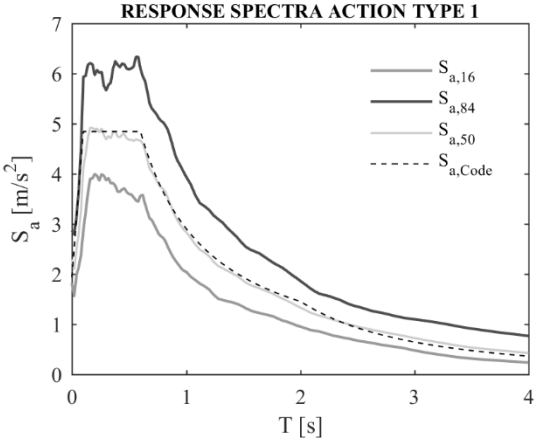

Figure 2 – Response spectra considered to be compatible with seismic action type 1

Finally, the discrete probability associated with the damage states are determined. The damage states (DSk with k=1,…,5) are defined to be conceptually compatible with the European Macroseismic Scale (EMS-98 (Grünthal, 1998)): DS0 – no damage, DS1 – slight damage, DS2 – moderate damage, DS3 – heavy damage, DS4 – very heavy damage, and DS5 – collapse. The discrete probability p_{DSk} for k=1,2 and 3, considering a given value of *im,* is defined by:

$$p_{DSk}(im) = p_{LSk}(im) - p_{LSk+1}(im) = \Phi\left(\frac{1}{\beta_{LSk}}\log\left(\frac{im}{IM_{LSk}}\right)\right) - \Phi\left(\frac{1}{\beta_{LSk+1}}\log\left(\frac{im}{IM_{LSk+1}}\right)\right) \tag{8}$$

p_{DS4} is generically named "complete" damage, including DS4 – very heavy damage and DS5 – collapse, resulting that $p_{DS4}=p_{LS4}$. This occurs because LS5 cannot be correctly capture by numerical models. However, assuming that the discrete probability distribution (p_{DS}) is represented by a binomial distribution, it is possible to obtain:

$$p_{DS5}(im) = 0.8\left[1-(1-0.14\mu_{DS}^{1.4})^{0.35}\right] p_{LS4}(im) \quad (9)$$

$$p_{DS4}(im) = p_{LS4}(im) - p_{DS5}(im) \quad (10)$$

$$\mu_{DS} = \sum_{1}^{4} p_{LSk} \quad (11)$$

Finally, the discrete probability p_{DS0} is calculated:

$$p_{DS0} = 1 - p_{LS1}(im) = \Phi\left(\frac{1}{\beta_{LS1}}\log\left(\frac{im}{IM_{LS1}}\right)\right) \quad (12)$$

Next, the criteria adopted for the analysis and derivation of the fragility functions associated with the global and local behaviour are described in detail in §3 and §4, respectively. As aforementioned, the fragility functions are evaluated individually and are then combined in order to define a single representative fragility curve, as defined in §6.

3. Analysis of the global behaviour

3.1 Modelling strategy

The global behaviour of URM buildings is based on the assumption that the connection between walls and the connection between walls and floors/roof are effective to prevent the occurrence of local mechanisms associated to the out-of-plane response and overturning of parts of the building. In this work, the global behaviour is analysed my means of three-dimensional models defined in TREMURI program (Lagomarsino, 2013). The commercial version of the program – 3Muri release 5.5.110 (http://www.stadata.com/) – is used to generate the equivalent frame idealization of URM walls while the research version – TREMURI (Lagomarsino, 2012) – is used to perform the non-linear analyses. The three-dimensional models are obtained by assembling: 1) the walls, modelled as an equivalent frame, and 2) the horizontal diaphragms (floors and roof), modelled as membrane elements.

Walls: equivalent frame model

The equivalent frame model approach comprehends the discretization of masonry walls with openings into a set of panels: 1) piers – vertical elements carrying both vertical and horizontal loads, 2) spandrels – horizontal elements coupling piers and limiting their end-rotations in case of horizontal loads, and 3) rigid nodes – undamaged elements confined between piers and spandrels.

The behaviour of the masonry panels (piers and spandrels) is modelled by non-linear beams characterized by a linear piecewise force-deformation constitutive law (Cattari and Lagomarsino, 2013a). This constitutive law is based on a phenomenological approach that aims to describe the non-linear response of masonry panels for increasing damage levels (DLi, with i=1,…,5) by assuming a progressive strength degradation (β_i) at predetermined drift levels (δ_i); these values can be easily defined basis on experimental data on URM panels and they can be properly differentiated in case of pier and spandrel elements. Each DLi represents the point after which the element experiences a damage state (DSk).

The response of the elements is determined from the comparison between the acting shear force (V) and the ultimate shear force (V_u) considering the occurrence of flexural or shear failure modes. The flexural behaviour of piers is defined according to the beam theory as proposed in EC8-1 (CEN, 2004) and Italian Code – NTC08 (2008). The flexural behaviour of spandrels is defined according to the criterion proposed by Cattari and Lagomarsino (2008) assuming an equivalent tensile strength on the elements due to the interlocking of the masonry units at the end section of spandrels. The shear behaviour of both piers and spandrels is governed by the diagonal cracking failure mode defined according to Turnšek and Čačovič (1970) and Turnšek and Sheppard (1980) Mixed failure modes are also possible, when the prediction between flexural and shear modes is close one to each other.

The linear piecewise constitutive law describes, in addition, the initial stiffness degradation of the panel by two parameters: 1) k_{in} which gives the ratio between the elastic (k_{el}) and the secant (k_{sec}) stiffness at the point where V_u is reached, and 2) k_0 which gives the ratio between the shear force at the end of the elastic phase and the ultimate shear force (V_u).

According to the equivalent frame idealization provided as default by 3Muri program, the connection between walls is defined by default as good quality. However, it is known that one of the main vulnerabilities of URM buildings are the connections between walls. To analyse the effect of the connections in the global behaviour of the buildings, the interface between walls has been modelled through link beams at the floor level, as exemplified in Figure 3 by properly modifying the automatic mesh resulting from the commercial version of the program. In this case, the properties of the link beams, namely the area (A) and inertia (I), are defined through an iterative procedure that aims to simulate the behaviour of connections. This procedure compares the global behaviour of the buildings in terms of pushover curves and maximum base shear force by considering as target reference the two limit cases of perfectly coupled and completely uncoupled walls.

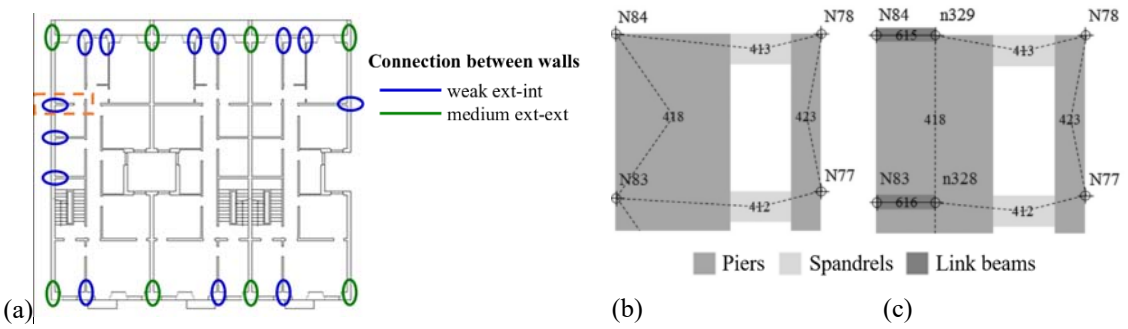

Figure 3 – Example of connection between walls: (a) identification of connections (plan view) and mesh of elements for the connection between exterior and interior walls (b) without and (c) with link beams

Horizontal diaphragms: membrane elements

Horizontal diaphragms are modelled as 3- or 4-nodes orthotropic membrane finite (plane stress) elements. These elements are characterized by the following equivalent parameters: thickness (t_{eq}), modulus of elasticity in the principal direction of the floor (spanning orientation) and in the perpendicular direction, respectively denoted as E_1 and E_2, and shear modulus (G_{12}). The modulus of elasticity represents the in-plane stiffness of the membrane along the two perpendicular directions and accounts, in addition, for the degree of connection between walls and horizontal diaphragms. The shear modulus determines the tangential stiffness of the diaphragm and the horizontal force distribution between walls.

3.2. Definition of the capacity by non-linear static analyses

Pushover analysis is a non-linear static analysis method where the structure is subjected to constant gravity loads and monotonically varying horizontal loads aiming to simulate the effect of the seismic action on the structure (CEN, 2004). The behaviour of the structure (multi-degree-of-freedom, MDOF, system) is described by the pushover curve that relates the base shear force (V_b) and the horizontal displacement of a control node or that assumed as representative of the structural response of the system (d), providing information about the stiffness, strength and displacement capacity.

The EC8-1 (CEN, 2004) recommends applying at least two distributions of lateral loads: uniform – proportional to the mass, and modal – proportional to the fundamental mode shape. Several authors do not recommend the use of a modal distribution for the analysis of URM buildings with flexible diaphragms, mainly due to the low mass participation involved in the first modes of vibration of the structure (Marino et al., 2018; Lourenço et al., 2011; Endo et al., 2017). A possible alternative is the use of the inverse-triangular load distribution – proportional to the product between the mass and the height of the node – because it assures that the seismic masses in all parts of the building are involved in the pushover analysis (Lagomarsino and Cattari, 2015; Cattari et al., 2015). Therefore, this work proposes to perform the non-linear static (pushover) analyses by considering a uniform and an inverse-triangular (named triangular for simplicity) load distributions. The analyses are performed in the two main directions of the building, including negative and positive orientation. The horizontal displacement represented in the pushover curve has been assumed as the average of the displacement of nodes located at the top floor, weighted on their corresponding mass. This is a heuristic approach useful to define a curve representative of the whole structure in case of buildings with flexible diaphragms and/or in plan irregularities (Lagomarsino and Cattari, 2015).

3.3. Definition of limit states thresholds

The EC8-3 (IPQ, 2017) recommends three limit states – damage limitation, significant damage and near collapse – which are directly defined on the pushover curve based on conventional displacement limits. Cattari and Lagomarsino (2013a) proposed, as an alternative, to define limit states, based on a multi-scale approach that correlates the damage level in the structure at three scales: 1) elements (piers and spandrels), 2) macro-elements (walls and horizontal diaphragms) and 3) global (represented by the pushover curve). The multi-scale approach is a heuristic procedure that aims to monitor the occurrence of significant damage in parts of the structure that may not be evident in the pushover curve in terms of strength degradation. A comparison between these approaches (IPQ, 2017; Cattari and Lagomarsino, 2013a) was carried out in (Simões et al., 2014). The difference between both criteria was particularly evident for the near collapse limit state. It was concluded that the thresholds were better defined by the second criterion (Cattari and Lagomarsino, 2013a), which is adopted here.

The damage levels in the structure (DLk, with k=1,…,4) are computed from the numerical models through the monitoring of proper engineering demand parameters. According to the multi-scale approach, the position of the DLk in the pushover curve is defined by the minimum displacement threshold obtained from the verification of conventional limits at the three scales. The following criteria are adopted in this work:

1. Element Scale – verification of the cumulative rate of damage in piers ($\Lambda_{P,DLk}$). This is defined as the percentage of piers that reached or exceeded given drift limits δ_{DLi}, weighted on the corresponding cross section (A_p), as:

$$\Lambda_{P,DLk} = \frac{\sum_p A_p H\left(\frac{\delta_p}{\delta_{DLi}} - 1\right)}{\sum_p A_p} \qquad \text{with } i = k + 1 \tag{13}$$

where the sum $\sum_P$ is extended to the total number of piers in the building, N_p (p=1,…,N_p), and H is the Heaviside function (equal to 0 until the demand δ_p in the s-th pier does not reach the capacity δ_{DLi} and equal to 1 after). The final threshold Λ_P is defined by Equation (14). This allows the spread of damage in a limited percentage of elements and avoids that threshold DLk is reached due to a single element (Cattari and Lagomarsino, 2013a). In particular, the proposed threshold takes into account the damage induced by the application of gravity loads ($\Lambda_{P,DLk,0}$) and the number of piers in the building (N_p).

$$\Lambda_P = 0.04 + \Lambda_{P,DLk,0} + \frac{2}{N_P} \tag{14}$$

2. Macro-Element Scale – verification of the cumulative damage of piers in a given wall and level ($\Lambda_{P,WL,DLk}$). This is defined as the maximum value of the minimum DLi attained in piers located in a given wall and level (WL), as proposed in Marino et al. (2018). The criterion is useful to detect when piers from a given level reached a DLi. Allowing for checking the occurrence of a soft-storey mechanism.
3. Global Scale – verification of the rate k_G of the total base shear over the maximum base shear force of the pushover curve (k_G=V/V_{max}). Rate k_G is assumed equal to 1.0 for DL2, 0.8 for DL3 and 0.6 for DL4. An additional verification avoids the positioning of PL1 and PL2 in the very beginning of the pushover curve: It is assumed that k_G should not be lower than 0.50 and 0.75, respectively.

The damage levels in the structure (DLk, with k=1,…,4) are considered to be coincident with the limit states (LSk, with k=1,…,4), which in turn are defined in terms of performance levels (PLk, with k=1,…,4). The three limit states in EC8-3 (IPQ, 2017) are assumed to correspond to performance levels PL2 to PL4, while PL1 is assumed to correspond to the operational limit state.

3.4. Computation of IM_{LS}

The intensity measure IM_{LS} is defined by the PGA that produces the attainment of the limit states LS (or PL). As stated, the Capacity-Spectrum Method with overdamped spectrum and without any iterative procedure (Lagomarsino and Cattari, 2015), is adopted. The computation of the intensity measure for the global behaviour IM_{LS} is based on the following steps:

1. Definition of the capacity curve by converting the pushover curve (MDOF system) into an equivalent SDOF system. The conversion is based on a transformation factor (Γ) computed as a function of a displacement shape vector, assumed to be consistent with the fundamental mode shape of the system, as proposed by Fajfar (2000). The transformation factor (Γ) is calculated according to Equation (15) where m_i and Φ_i are, respectively, the mass and modal displacement (normalized to the roof level) in each node i of the structure and m^* is the mass of the equivalent SDOF system. The base shear force (V^*) and the displacement (d^*) of the equivalent SDOF system are computed according to Equation (16). The capacity curve is plotted in spectral coordinates, i.e. spectral acceleration (S_a) as a function of spectral displacement (S_d), assuming the equivalences presented in Equation (17).

$$\Gamma = \frac{\sum m_i \Phi_i}{\sum m_i \Phi_i^2} = \frac{m^*}{\sum m_i \Phi_i^2} \tag{15}$$

$$V^* = V_b / \Gamma \quad \text{and} \quad d^* = d / \Gamma \tag{16}$$

$$S_a = V^* / m^* \quad \text{and} \quad S_d = d^* \tag{17}$$

2. Determination of the equivalent viscous damping (ξ_{PL}) and period (T_{PL}) in the capacity curve, according to Equation (5) and (3), respectively. The hysteretic damping (ξ_h) is estimated based on cyclic pushover analyses by considering as target the displacement limit state threshold D_{PL}, and is related to the area enclosed by the full hysteresis loops as:

$$\xi_h = \frac{E_D}{2\pi E_0} \tag{18}$$

where E_D is the energy dissipated by the structure during the cyclic response and E_0 is the total strain energy. According to (Cattari and Lagomarsino, 2013a) this estimation of the equivalent viscous damping allows to take into account the seismic behaviour, being a better estimation than analytical expressions proposed in literature, since is targeted on the specific building under investigation.

3. Definition of the seismic demand in an acceleration-displacement response spectrum (ADRS) format. The elastic response spectrum is normalized, S_{d1}, so that $S_a(S_d=0)=1$, and reduced by the damping correction factor (η), given by Equation (4).
4. Computation of the PGA for which the seismic displacement demand (S_d) is equal to the displacement capacity of the equivalent SDOF (d^*) for a specified PL, according to Equation (2).

Figure 4 exemplifies the capacity curve and the overdamped response spectra, in spectral coordinates, used for the computation of the PGA values compatible with the four performance levels.

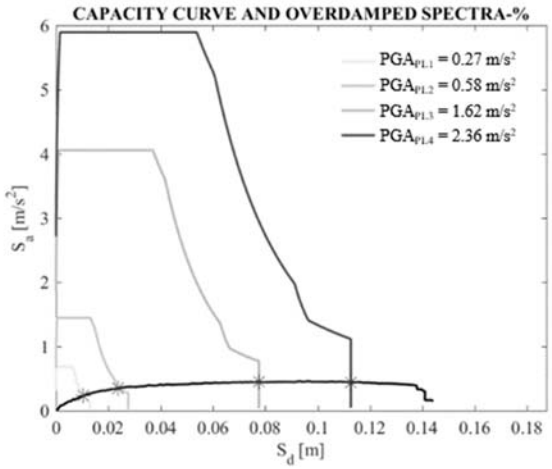

Figure 4 – Computation of the PGA values compatible with the four performance levels

4. Analysis of the local behaviour

4.1. Modelling strategy

URM buildings under seismic actions are particular prone to local failure modes related to the out-of-plane response and overturning of façade walls insufficiently connected to the rest of the structure and standing out elements, such as gable walls, parapets and chimneys. The identification of possible local mechanisms is supported on damage observation of URM buildings after past earthquakes (D'Ayala and Paganoni, 2009; Penna et al., 2014) and from experimental tests (Lourenço et al., 2011; Candeias, 2008). The activation of local mechanisms depends of the quality and strength of the connections between the façade walls and elements such as side walls, partition walls, floors and roof structure. In case specific measures have been implemented to prevent the overturning of the façade walls, for example with the introduction of tie-rods or ring beams at the floor level, out-of-plane mechanisms relying on arch effect (flexural mechanisms) may also occur. Standing out elements (e.g. gable walls, parapets and chimneys) are very vulnerable to overturning even for low intensity seismic actions. More than one mechanism can occur and sometimes it is not easy to select in advance the most dangerous; in these cases, all possible mechanisms must be investigated (Lagomarsino, 2015).

4.2. Definition of the capacity by non-linear kinematic analyses

Non-linear kinematic analyses are based on the assessment of the work done by equilibrated forces applied to a set of compatible generalized virtual displacements (Lagomarsino, 2015). The response of the mechanism is described by a curve that relates the static seismic multiplier (α) with the incremental horizontal displacement of a control node (d_C). This curve may be regarded as equivalent to the pushover curve obtained for the global seismic behaviour.

4.3. Definition of limit state thresholds

The displacement thresholds proposed in (Lagomarsino, 2015) are adopted in this work and defined directly on the capacity curve of the mechanism. The displacement thresholds associated with DL1 and DL2 are coincident, respectively, with the limit of the elastic behaviour ($d_{DL1} = d_e$) and the point of rocking activation ($d_{DL2} = d_s$). DL3 and DL4 are defined as a function of displacement where the capacity curve is zero (d_0), point in which overturning occurs. The displacement associated with DL4 (d_{DL4}) is assumed equal to $0.4d_0$, in order to be coherent with the definition of near collapse limit state. As to DL3, it is assumed before DL4 ($d_{DL3} = 0.25d_0$) and after checking that no failure of important connections occurs (e.g. unthreading of rafters or beams).

4.4. Computation of IM_{LS}

The Capacity-Spectrum Method with overdamped spectrum is adopted with an iterative procedure (Degli Abbati, 2014). The latter is necessary in case the local mechanism is located in the upper level of the building to properly consider the dynamic filtering effect of the main structure that produces an amplification of the seismic demand. This depends on the non-linear behaviour of the main structure, as illustrated more in detail in the following. The computation of the intensity measure for the local behaviour IM_{LS} is based on the following:

1. Definition of the capacity curve by converting the curve that relates the static seismic multiplier (α) with the incremental horizontal displacement of a control node (d_C). The conversion is based on a transformation factor (Γ) and assuming that each block is defined by lumped masses at their barycentre. Equation (19) provides the definition of the capacity curve in spectral acceleration (S_a) and displacement (S_d) coordinates.

$$S_a = \frac{g\alpha(d^*)}{e^*} \quad \text{and} \quad S_d = d^* = d_C / \Gamma \tag{19}$$

where e^* is the rate of total mass that participates in the mechanism, given by Equation (20), and Γ is the transformation factor given by Equation (21).

$$e^* = \frac{\left[\sum_{k=1}^{n_b}(W_k + Q_k)\delta_{Qx,k}\right]^2}{\left[\sum_{k=1}^{n_b}(W_k + Q_k)\right]\left[\sum_{k=1}^{n_b}(W_k + Q_k)\delta_{Qx,k}^2\right]} \tag{20}$$

$$\Gamma = \frac{\delta_{Cx}\sum_{k=1}^{n_b}(W_k + Q_k)\delta_{Qx,k}}{\sum_{k=1}^{n_b}(W_k + Q_k)\delta_{Qx,k}^2} \tag{21}$$

Here, n_b is the number of blocks (with k=1,…,n_b), W_k is the weight of block k plus the masses it carries during the activation of the kinematism, Q_k is the total weight of masses that are not carried by block k but are connected to it during the activation of the kinematism (e.g. the weight of the roof), $\delta_{Qx,k}$ is the virtual horizontal displacement of the barycentre of weights W_k and Q_k, assumed positive in the direction of the seismic action that activates the kinematism and δ_{Cx} is the horizontal component of the virtual displacement of the control node.

2. Definition of an initial pseudo-elastic branch in the capacity curve to describe the dynamic response of the considered part of the structure before the activation of the kinematism, in accordance to the formulation of the bi-linear model (Lagomarsino, 2015; Doherty et al., 2002), which produces overturning conditions similar to the Housner model (Housner, 1963). The bi-linear model is defined by two distinct periods: the elastic period (T_e) and the secant period (T_s). The capacity curve is expressed by:

$$S_a(d^*) = \begin{cases} \dfrac{4\pi^2}{T_e^2}d^* & d^* \le d_e \\ \dfrac{4\pi^2}{T_e^2(1-d_e/d_s)}d_e\left[1-\dfrac{d^*}{d_s}-\dfrac{T_e^2}{T_s^2}\left(1-\dfrac{d^*}{d_s}\right)\right] & d_e < d^* < d_s \\ \dfrac{g\alpha(d^*)}{e^*} & d^* \ge d_s \end{cases} \tag{22}$$

where, d_e and d_s are, respectively, the displacements corresponding to T_e and T_s. In this work, the elastic period (T_e) is calculated by approximation to the period of a cantilever beam. The secant period (T_s) is estimated assuming that the secant stiffness is 50% of the elastic stiffness. The secant displacement is obtained by the intersection with the descending branch of the capacity curve (rocking activation).

3. Determination of the equivalent viscous damping (ξ_{PL}) and period (T_{PL}) in the capacity curve, according to Equation (23) and (3), respectively. The hysteretic damping (ξ_h) is assumed equal to 7% following the experimental results in (Lagomarsino 2015; Degli Abbati and Lagomarsino, 2017).

$$\xi(d^*) = \begin{cases} \xi_{el} & d^* \le d_e \\ \xi_{el} + \xi_h\left(1-\dfrac{d_e}{d^*}\right) & d^* > d_e \end{cases} \tag{23}$$

4. Definition of the seismic demand in an acceleration-displacement response spectrum (ADRS) format. In case the local mechanism is located in the upper level of the building, it is necessary to adopt a floor response spectrum that takes into account the dynamic filtering effect of the structure. It is proposed to define the floor response spectrum according to the formulation in (Degli Abbati, 2016; Degli Abbati et al., 2018) which takes into account the dynamic parameters of all the relevant modes of the main

structure. The computation of the acceleration response spectrum at position Z of the main structure ($S_{a,Z}$), where the mechanism of period T and equivalent viscous damping ξ is located, is given by:

$$S_{a,Z}(T,\xi) = \sqrt{\sum_{k=1}^{N} S_{aZ,k}^2(T,\xi)} \qquad (\geq S_a(T)\eta(\xi) \quad \text{for} \quad T > T_1) \tag{24}$$

where η is the damping correction factor defined by Equation (4), $S_{aZ,k}(T,\xi)$ is the acceleration response spectrum at position Z due to k^{th} mode of the N modes of the main structure considered, defined according to:

$$S_{aZ,k}(T,\xi) = \begin{cases} \dfrac{AMP_k PFA_{Z,k}}{1+\left(AMP_k-1\right)\left(1-\dfrac{T}{T_k}\right)^{1.6}} & T \leq T_k \\ \dfrac{AMP_k PFA_{Z,k}}{1+\left(AMP_k-1\right)\left(\dfrac{T}{T_k}-1\right)^{1.2}} & T > T_k \end{cases} \tag{25}$$

where AMP_k is the factor of amplification, defined by Equation **Erro! A origem da referência não foi encontrada.**, while $PFA_{Z,k}$ is the peak floor acceleration, defined by Equation **Erro! A origem da referência não foi encontrada.**:

$$AMP_k = f_k f_s \tag{26}$$

$$PFA_{Z,k} = S_a(T_k)\eta(\xi_k)\left|\Gamma_k \phi_k\right|\sqrt{1+4\xi_k^2} \tag{27}$$

The amplification factor AMP_k in Equation (26) collects two contributions: f_k that depends on the viscous damping of the main structure, and f_s that depends on the viscous damping of the mechanism. In Equation (27), $S_a(T_k)$ is the acceleration of the ground motion at period T_k of the main structure, ξ_k is the equivalent viscous damping of the main structure, Γ_k and ϕ_k are the modal participation coefficient and the modal shape of mode k. The modal participation coefficient (Γ_k) is calculated according to Equation (28), considering the modal mass (m_i) and displacement (Φ_i) mobilized in the k^{th} mode in each node i of the main structure. The modal shape (ϕ_k) of mode k is evaluated after the normalization to the maximum horizontal displacement of the main structure. As it is indicated by the condition in brackets in Equation (24), for long periods, the floor spectrum has to be taken always greater than the response spectrum of the ground motion.

$$\Gamma_k = \frac{\sum m_i \Phi_i}{\sum m_i \Phi_i^2} \tag{28}$$

5. Development of an iterative procedure to compute the overdamped floor response spectrum associated with PL. This aims to guarantee coherence between the damping properties at the global and local scales and to establish a limit for the seismic verification at the local scale taking into account the progression of damage at the global scale. The following steps are considered:
   i. Definition of the period of the main structure ($T_{k,PL}$) based on the results from the non-linear static (pushover) analyses of the building in the direction of the out-of-plane mechanisms and corresponding equivalent viscous damping ($\xi_{k,PL}$).
   ii. Definition of the floor response spectrum.
   iii. Determination of the maximum PGA compatible with PL from the comparison between the capacity curve of the mechanism and the floor response spectrum.
   iv. Comparison of the maximum PGA compatible with PL at the local scale with the corresponding PGA at the global scale: a) if $PGA_{PL,L} > PGA_{PL,G}$, then the seismic verification at the global scale prevails (i.e. the building is no longer usable, even if the mechanism is verified), b) if $PGA_{PL,L} \leq PGA_{PL,G}$, then update $T_{k,PL}$ and $\xi_{k,PL}$ and repeat steps ii) to iv) until the process converges.

As an example, Figure 5 compares a ground response spectrum (S_a) with the floor response spectrum at the base of the last floor of a building (S_{aZ}) considering the filtering effect of the structure and the contribution of higher modes: $S_{aZ,2a}$ and $S_{aZ,2b}$. These modes correspond to the translation of the structure in the direction of the out-of-plane mechanism (Simões et al. 2019b). It is visible that, in this case, mode 2a has the main contribution to the floor response spectrum.

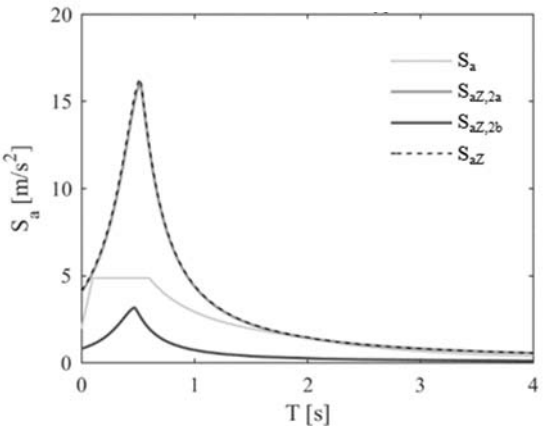

Figure 5 – Comparison between the ground response spectrum (S_a) and the floor response spectrum at the base of the last floor of the building (S_{aZ}) considering the filtering effect of the structure and the contribution of higher modes: $S_{aZ,2a}$ and $S_{aZ,2b}$

5. The URM "gaioleiro" buildings

5.1. Main features

The buildings constructed in the area of "Avenidas Novas" represent the core of the urban development of Lisbon in the transition between the 19th and 20th centuries. The main architectonical and structural features of these buildings are described in Simões et al. (2017). The buildings have between four and six stories, façade walls made of rubble masonry, side and interior walls made of brick masonry. Floors and roof are made of timber elements. The "gaioleiro" buildings may be subdivided into different types as a function of the dimension of the lot and the position of the building in the aggregate (Appleton, 2015). Previous works compared the seismic behaviour of the building types identifying the most vulnerable and most common type (Simões et al., 2014; Simões et al. 2018), which is adopted in this work.

5.2. Definition of a prototype building

The main geometric features of these buildings are identified based on the information available in the literature and on a detailed survey (Simões et al., 2016). The plan and front view of this prototype building are presented in Figure 6.

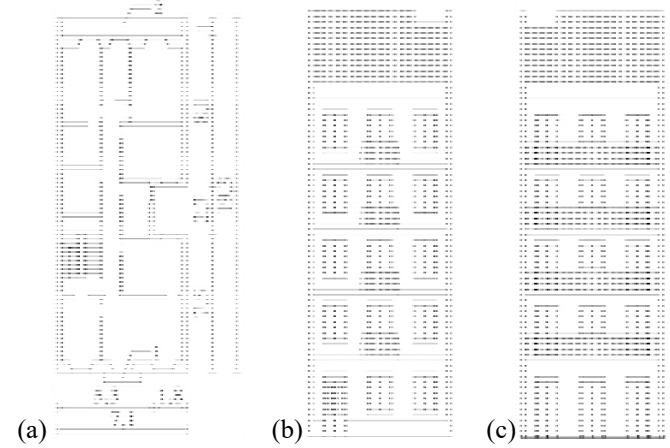

Figure 6 – Typical prototype building: (a) plan of the regular floors with dimensions in meters (1 – stone balcony in the street façade and 2 – jack arch balcony with steel profiles in the rear façade), (b) street façade and (c) rear façade

The typical building is five storeys high, characterized by small size façade walls and one flat per floor. The building structure is regular in elevation and irregular in plan due to the presence of a vertical airshaft close to one of the side walls. The ceiling height and the ventilation box height adopted follow (RSEU, 1903): the ventilation box has 0.60 m height, the ground floor and the first floor have 3.25 m, the second floor has 3.00 m, the third floor has 2.85 m and the fourth floor has 2.75 m. The prototype has 17 m total height.

The façade walls are made of rubble stone masonry and lime mortar, with 0.60 m of thickness at the ground floor and the thickness decreases 0.05 m in each floor. The wall below the windows is made of clay brick masonry and

lime mortar with 0.27 m of thickness. Above the windows there are clay brick relieving arches and lintels. The side walls and the airshaft walls are made of clay brick masonry and lime mortar with 0.27 m of thickness.
The interior walls are made of clay brick masonry or have a timber structure (walls made of vertical timber boards and horizontal laths filled in the gaps by rubble masonry). The main load-bearing walls are placed parallel to the façades to support the floor timber beams. Other walls are partition walls. The thickness of the interior clay brick masonry walls is: 0.15 m for main walls and 0.10 m for partition walls.
The floors and roof are made of timber elements: *Pinus pinaster Ait.* wood type. The main joists are set perpendicular to the façades with a distance of 0.40 m between each other. The joists have 0.18 m of height and 0.07 m of width, while the floor boards have 0.022 m of thickness. The pitched roof structure is supported on purlins disposed parallel to the façade walls.
The typical building is located in the middle or in the end of a row of buildings. A group of three equal buildings is considered to evaluate the effect of the aggregate in the seismic behaviour.

5.3. Involved uncertainties

Different classes of buildings have been identified in previous works (Simões et al., 2018; Simões, 2018). The differences are related to specific features that may affect the seismic behaviour of the buildings, such as geometry variations at the ground floor level, constructive details and materials attributed to the structural elements. In this work, these variations are considered as epistemic uncertainties (related to the incomplete knowledge). The counterpart article (Simões et al., 2019a) presents the main features of the classes of buildings, compares their seismic behaviour and provides the final fragility curves for this class of tall URM buildings. Whereas, this section addresses one class of buildings aiming to illustrate the procedure for the derivation of the fragility functions associated with the in-plane and out-of-plane behaviour.
The class of buildings is characterized by: 1) ground floor level used as house, meaning that the structure is regular in elevation as all floors have the same configuration, 2) the side walls are shared between adjacent buildings, 3) the side walls are made of solid clay brick masonry, 4) the main interior walls are made of solid brick masonry, and 5) the partition walls are made of hollow brick masonry. A three-dimensional model of the building is defined in TREMURI program (Figure 7) starting from the prototype building (§5.2). As stated, a group of three buildings is adopted to consider: 1) the effect of the adjacent buildings and, 2) the fact that the side walls are shared between buildings, filled walls as shown in Figure 7 (b). Thus, the uncertainties associated are related to: 1) the identification of possible local mechanisms, and 2) to the variability in the definition of the capacity (β_C) for the global and local behaviour and consequently to the definition of the individual fragility functions.

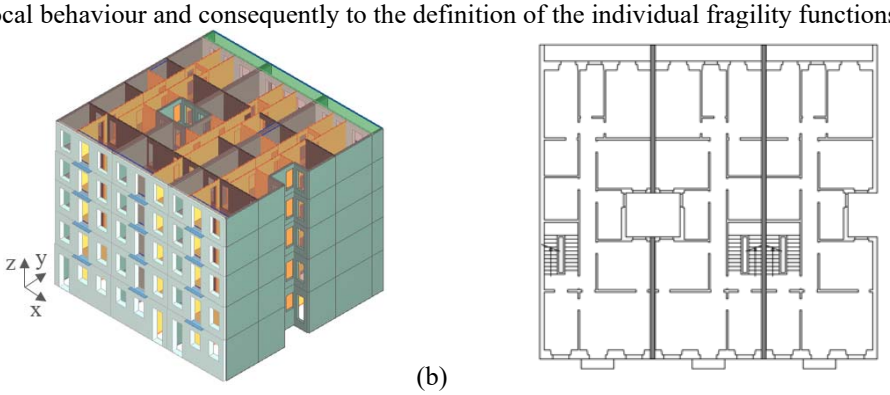

(a) (b)

Figure 7 – Adopted building for analysis: (a) three-dimensional model and (b) plan view

5.3.1. Identification of local mechanism and epistemic uncertainties

The analysis comprehends the identification of possible the out-of-plane mechanisms. These are defined based on the geometry of the building, layout of openings, constructive details and restraints given by the structure. It is reasonable to consider the collapse involving only the upper level of the façade walls, as proposed in (Simões et al., 2014). The façade is very slender (17 m height with decreasing thickness) but there are restraints that prevent the global overturning of the street façade wall, namely the connection to the side walls and the orientation of the timber floors perpendicular to the façade walls. This hypothesis is also supported by experimental results from shaking table tests on reduced scale building models (Lourenço et al., 2011; Candeias, 2008). These local mechanisms are also more likely to occur on the street façade than on the rear façade due to the presence of the jack arch balconies with steel profiles.
After analysing the constructive details of the last floor (Figure 8), three out-of-plane mechanisms are considered (Figure 9): the overturning of the central pier, with a plastic hinge at the base (Mech. 1), the flexural mechanism of the central pier, with a plastic hinge at the base and a plastic hinge separating the pier in two blocks (Mech. 2), and the overturning of the parapet, with a plastic hinge at the base (Mech. 3).

Concerning Mech. 1, the two central piers are more vulnerable to overturning than the lateral piers, as they are connected to the side walls. The lintels that link lateral and central piers are very slender and prone to rotate around a vertical axis with torsional sliding on the masonry joints (the friction contribution is close to zero because the vertical loads are low at this level). From the configuration of the street façade wall (Figure 8 (a)), the central piers have a door on one side and a window on the other; the possible restraint provided by the masonry panel below the window is neglected due to its lower thickness (0.27 m). The roof timber structure is placed perpendicular to the façade walls and aligned with the central piers (Figure 8). Assuming that the timber roof structure is connected to the interior walls and simply supported on the façade walls, in case of the overturning of the central piers, the timber elements will slide and unthread, transmitting a stabilizing horizontal force to the piers due to the friction originated in the contact surface. This force is equivalent to the vertical load transmitted by the roof to the piers (P_R) multiplied by the coefficient of friction (μ).

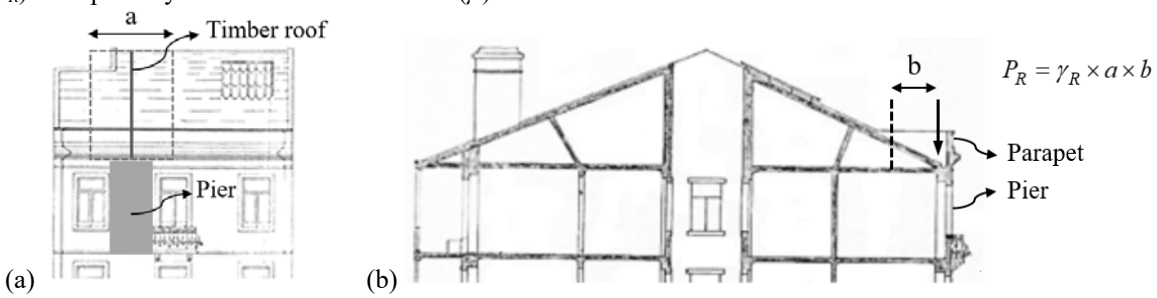

Figure 8 – View from the last floor of the buildings: (a) street façade wall and (b) section cut

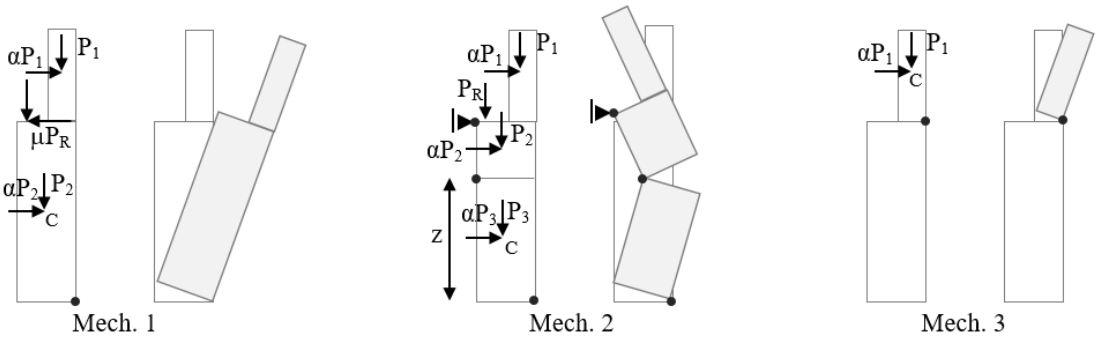

Figure 9 – Configuration and actions involved in the mechanisms: Mech. 1 – overturning of the central pier, Mech. 2 – flexural mechanism of the central pier and Mech. 3 – overturning of the parapet

The development of Mech. 2 is supported on the hypothesis that the horizontal displacement on top of the central piers is restrained due to the effect of strengthening, due to the insertion of tie-rods connecting the central piers to the interior walls or the introduction of a beam at the top of the wall. Then, flexural mechanism of the central piers is determinant (Griffith et al., 2004; Mendes et al., 2014). Overturning of the parapet may also occur (Mech. 3), unless these elements are restrained.

Figure 9 identifies the actions involved on the three mechanisms: P_1, P_2 and P_3 are, respectively, the parapet and central pier self-weight, P_R is the weight of the roof transmitted to the pier (determined according to Figure 8), α is the coefficient proportional to the vertical loads that induces the loss of equilibrium of the system and activates the kinematism, denoted as the static seismic multiplier. This multiplier is determined by evaluating the work done by equilibrated forces on a set of compatible generalized virtual displacements.

The occurrence of one or more mechanisms depends on the condition of the building, possible strengthening interventions to prevent the simple overturning of the central piers and parapets. In this regard, the local behaviour of the buildings may be analysed by considering two different scenarios:

1. The last floor of the buildings, with the hypothesis of: i) simple overturning of the central piers (Mech. 1) or ii) flexural mechanism of the central piers (Mech. 2).
2. The parapet, with the hypothesis of: i) simple overturning (Mech. 3) or ii) no problem, in case a strengthening solution has been implemented or in case the building has no parapet.

Each scenario is assumed as an epistemic uncertainty and treated by the logic-tree approach, as presented in Figure 10. An expert judgement probability is attributed to each branch of the tree to quantify the reliability of the different options. In what concerns the first scenario, a lower probability is defined for Mech. 2 considering that the flexural mechanism only occurs in case a strengthening solution has been implemented. Thus, it is assumed that in 70% of the cases Mech. 1 may occur, while only in 30% of the cases Mech. 2 may occur. In what concerns the second scenario, it is assumed that in 60% of the cases Mech. 3 may occur, while in 40% there is no problem

(meaning that either the parapet does not exist or has been strengthened and will not collapse). In this point, it is important to note that the overturning of the parapet to the street is relevant from the point of view of life safety, however from the point of view of the performance limit state of the main building, it represents the possible damage of a non-structural element.

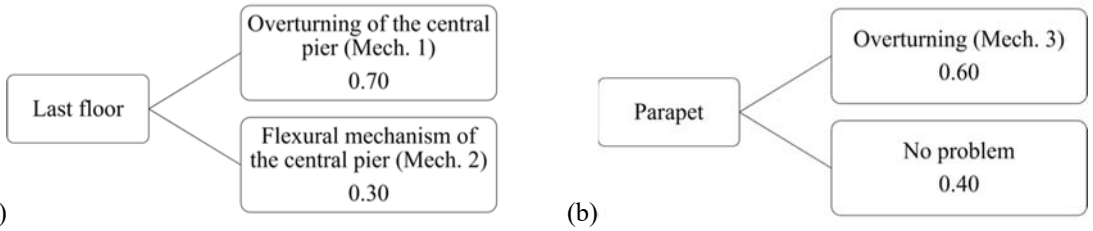

Figure 10 – Local behaviour scenarios: (a) last floor of the building and (b) parapet

5.3.2. Identification of aleatory uncertainties

The variability in the definition of the capacity (β_C) aims to account for the uncertainties in the quantification of the variables and the intrinsic scatter, as stated in §2. Different aleatory variables are considered for the analysis of the global and local behaviour. Each aleatory variable is defined within a plausible interval of values, based on the information available in the literature and results from tests.

Global behaviour

The aleatory variables are treated by the Monte Carlo Method (Rubinstein, 2011). Each aleatory variable is described by an appropriate continuous probability density function ($f_X(x)$) characterized by median value ($X_{k,med}$) and dispersion (β) so that the 16% and 84% percentiles of the distribution correspond, respectively, to the lower ($X_{k,low}$) and upper ($X_{k,up}$) values of the range of variation. An alternative procedure to the 16% and 84% percentiles is to consider the coefficient of variation, as suggested in the Probabilistic Model Code (JCSS, 2011).

Monte Carlo simulations are used to define possible outcome values for each aleatory variables X_k. If M is the number of Monte Carlo simulations, M models are defined in which each aleatory variable X_k assumes the M outcome value. The number of simulations is defined in order to have a sufficient number of results to reach a good estimation of the parameters that define fragility functions for the building class (see (Simões et al., 2019a) for additional details).

The variability in the definition of the capacity for the global behaviour (β_C) is defined as follows:

1. For each model M, determination of the intensity measure $IM_{LS,G}$ that produces the attainment of limit state threshold LS according to Equation (2).
2. Sort the IM_{LS} values in ascending order.
3. Attribution of an equal probability p to each $IM_{LS,G}$ values, with p=1/M.
4. Calculation of the median value IM_{LS} and dispersion β_C assuming that the IM_{LS} values are lognormal distributed.

The aleatory variables for the analysis of the global behaviour account for variations on the mechanical properties of masonry, strength and deformability characteristics of masonry piers and spandrels, mechanical properties of interior timber walls, quality of connections between walls and in-plane stiffness of timber floors. Table 1 characterizes the aleatory variables considered in terms of probability density function, median value ($X_{k,med}$) and dispersion (β). A total of 50 aleatory variables are considered, divided in 17 groups. Lognormal distributions are attributed to the aleatory variables varying between]0,+∞[, while beta distributions are attributed for those varying between [0,1] or having, from a physical point of view, a range of variation equal to one.

Group 1 and 2 (rubble stone masonry), Group 3 and 4 (solid brick masonry) and Group 6 and 7 (hollow brick masonry) define the mechanical properties of masonry. The interval of values is defined from the application of the Bayesian update approach (Bracchi et al., 2016; Franchin and Pagnoni, 2018). The Bayes' Theorem is used to update the probability of *a priori* distribution given that new evidences are available. In this case, the *a priori* distribution is defined by the interval of values proposed in the commentary to the NTC08 (MIT, 2009) for the relevant masonry types, whereas the new evidences are defined by the experimental test results carried out in Lisbon, including in situ and laboratory tests (Simões et al., 2017; Simões, 2018).

Group 5, 8 and 11 refer to the modelling of the flexural behaviour of spandrels according to the criterion proposed in (Cattari and Lagomarsino, 2008) assuming an equivalent tensile strength on the elements due to the interlocking of the masonry units at the end section of spandrels (*Int* – ratio between length and height of the masonry unit). For brick masonry, *Int* is equal to 2 (deterministic value). For rubble stone masonry, lower values are expected due to the masonry irregularity (Group 11). Another input is the coefficient of friction in the mortar joints in the end section of spandrels (μ_{loc} – Group 5, 8 and 11).

Groups 9 and 10 characterize the mechanical properties of spandrels in the façade walls. Considering that these panels may be made of rubble stone masonry or clay brick masonry, the properties attributed, range between the mechanical properties of the two types of materials.
Groups 12, 13 and 14 are related to the formulation of the linear piecewise constitutive law associated with the initial stiffness degradation (k_{in} and k_0) and the progressive degradation of strength (δ_i and β_i) of the panels.
The values for Groups 12 and 13 are defined based on experimental test results (Kržan et al., 2015; Haddad et al., 2017; Vanin et al., 2017) and expert judgement. For instance, in case of piers, the ultimate drift levels (DL4) reflect the recommendations from structural codes (NTC, 2008; IPQ, 2017): between 0.4% and 0.6% in case of shear failure and between 0.8% and 1.2% in case of flexural failure. In case of spandrels, the experimental results from (Beyer and Mangalathu, 2014) are taken into account to characterize the behaviour of the shallow brick arches present in the façade walls (faç) and of the timber elements in the clay brick masonry walls. For spandrels with shallow brick arches, DL3 threshold is not defined in terms of drift, but in terms of ductility (μ), considering the greater deformation capacity of the elements observed during the experimental tests (Beyer and Mangalathu, 2014). Due to the limited information available, the same intervals of values are adopted for the different types of masonry.
In what concerns Group 14, structural codes (IPQ, 2010; NTC, 2008) recommend adopting a 50% reduction of the elastic stiffness properties (corresponding to $k_{in} = 2$), unless more detailed information is available. Previous parametrical studies have indicated this level of reduction leads to conservative estimate of the non-linear behaviour of the panels (Cattari and Lagomarsino, 2013b; Calderini et al., 2009). Therefore, it is proposed to vary k_{in} between 1.00 and 1.50, in order to simulate the extreme cases in which there is no stiffness degradation and the case in which this reduction is approximately 67% due to the expected cracked state of the buildings. As to k_0, it is proposed to consider a range between 0.50 and 0.80.

Table 1 – Characterization of aleatory variables in terms of distribution of probability, median value and dispersion

Description	Group	X_k	Distribution	$X_{k,med}$	β
Rubble stone masonry	1	E-G-f_c [MPa]	Lognormal	736.50-245.50-0.95	0.18-0.18-0.12
	2	τ_0 [MPa]	Lognormal	0.022	0.18
Solid clay brick masonry	3	E-G-f_c [MPa]	Lognormal	840.65-280.22-1.07	0.16-0.16-0.11
	4	τ_0 [MPa]	Lognormal	0.074	0.21
	5	μ_{loc}	Lognormal	0.53	0.28
Hollow clay brick masonry	6	E-G-f_c [MPa]	Lognormal	840.65-280.22-0.87	0.16-0.16-0.14
	7	τ_0 [MPa]	Lognormal	0.074	0.21
	8	μ_{loc}	Lognormal	0.53	0.28
Spandrels in façade walls	9	E-G-f_c [MPa]	Lognormal	779.10-259.70-1.00	0.24-0.24-0.17
	10	τ_0 [MPa]	Lognormal	0.041	0.82
	11	Int-μ_{loc}	Lognormal	1.00-0.53	0.69-0.28
Drift and residual strength thresholds for piers	12	δ_{F3}-δ_{F4}-δ_{F5}	Lognormal	0.0058-0.0098-0.0147	0.24-0.22-0.20
		δ_{S3}-δ_{S4}-δ_{S5}	Lognormal	0.0029-0.0049-0.0069	0.24-0.22-0.20
		β_{F4}-β_{S3}-β_{S4}	Beta	0.85-0.70-0.40	0.05-0.10-0.15
Drift, residual strength and ductility thresholds for spandrels	13	δ_{F3}-δ_{F4}-δ_{F5}	Lognormal	0.0019-0.0058-0.0194	0.24-0.25-0.25
		δ_{S3}-δ_{S4}-δ_{S5}	Lognormal	0.0019-0.0058-0.0194	0.24-0.25-0.25
		β_{F4}-β_{S3}-β_{S4}	Beta	0.55-0.55-0.55	0.15-0.15-0.15
		β_{F4}-β_{S3}-β_{S4} |faç	Beta	0.40-0.40-0.40	0.20-0.20-0.20
		μ |faç	Beta	4.20	0.99
Stiffness degradation of masonry panels	14	k_{in}-k_0	Beta	0.65-0.50	0.15-0.25
Timber walls	15	E-G-f_c [MPa]	Lognormal	109.54-1.73-0.54	0.60-0.55-0.29
Link beams	17	A-I [m^2-m^4]	Lognormal	0.0004-0.0002	0.81-0.81
Stiffness of timber floors	16	G [MPa]	Lognormal	9.88	0.48

E – modulus of elasticity, G – shear modulus, f_c – compressive strength, τ_0 – equivalent shear strength, μ_{loc} – coefficient of friction on the mortar joints in the end section of spandrels, Int – interlocking of the masonry units in the end section of spandrels, δ_{Si} – drift limit for the shear behaviour at damage level i, δ_{Fi} – drift limit for the flexural behaviour at damage level i, β_{Si} – residual strength for the shear behaviour at damage level i, β_{Fi} – residual strength for the flexural behaviour at damage level i, μ – ductility of the brick arch for damage level 3, k_{in} – ratio between the initial and the secant stiffness, k_0 – ratio between the elastic strength and the ultimate strength, A – area of the link beams and I – inertia of the link beams

Group 15 quantifies the mechanical properties of the interior timber “walls. The mechanical properties of these walls are determined based on the experimental results from compression and shear tests performed by Rebelo et al. (2015). Group 16 defines the area (A) and inertia (I) of the link beams that set the connection between perpendicular exterior walls (Figure 3). These connections are defined as medium quality connections justified by the use of different materials between façade walls (rubble stone masonry) and side walls (brick masonry). The connection between exterior walls and interior clay brick masonry walls are defined as weak quality connections taking into account that the interior walls were constructed after exterior walls. The properties of the link beams representative of the weak quality connections are assumed as deterministic. Group 17 characterizes the flexible behaviour of timber floors, represented by the shear modulus (G) of an equivalent finite membrane element with 0.022 m of thickness, corresponding to the thickness of the timber boards. The range of variation is defined in (NZSEE, 2017), which proposes reference values as a function of the floor system and state of conservation, based on (Giongo et al., 2013).

The Monte Carlo simulations are defined for each variable starting from the continuous probability density function attributed and considering additional correlations between variables, as described in the following. It is assumed that within the 17 groups, the aleatory variables are fully correlated in order to guarantee a positive linear relationship between the variables attributed to the same model (correlation coefficient, R = +1). A negative linear correlation (R = –1) is considered for Group 14 related to the initial stiffness degradation of the masonry panels. This aims to define two extreme behaviours for the transition between elastic and plastic phases. Thus, for higher initial stiffness degradation (higher value of k_{in}) a lower value of k_0 is expected, so to have a longer interval between the first cracks and the reaching of the ultimate strength capacity (the opposite relation is also valid). It is also proposed to assume a correlation coefficient of 0.5 between Group 1 and 2, Group 3 and 4, Group 6 and 7 and Group 9 and 10, taking into account that the modulus of elasticity (E), the shear modulus (G) and the compressive strength (f_c) are not fully correlated nor uncorrelated with the equivalent shear strength (τ_0).

Local behaviour

The aleatory variables are treated by the Response Surface Method (Liel et al. 2009; Ottonelli et al., 2015). Each aleatory variable is described by a lower ($X_{k,low}$), median ($X_{k,med}$) and upper ($X_{k,up}$) values. This method is based on the approximation of the hyperplane that fits the response surface of the variable log(IM_{LS}) in the hyperspace of the normalized variables representing the aleatory variables considered. The angular coefficients (β_{Ci}) defining the hyperplane are determined according to:

$$\beta_{Ci} = (Z^T Z)^{-1} Z^T Y \tag{29}$$

where, Z is a matrix, with M rows x N columns (where $M=2^N$ is the number of models defined by the full factorial combination and N is the number of aleatory variables), which collects the corresponding normalized variables (equal to –1 for $X_{k,low}$ and +1 for $X_{k,up}$) and Y is a vector, with M rows, which collects the corresponding log(IM_{LS}) values. The variability in the definition of the capacity of the local mechanism (β_C) is given by:

$$\beta_C = \sqrt{\beta_{Ci}^T \beta_{Ci}} \tag{30}$$

The aleatory variables for the analysis of the local behaviour account for the geometry of the blocks involved in the mechanisms and the value of the external forces applied. Although the geometry of the building is considered deterministic, for the analysis of the local behaviour, the thickness of the parapet ($t_{parapet}$) and the thickness of the central pier (t_{pier}) are considered aleatory variables as the behaviour of the mechanisms is mainly influenced by the geometry of the blocks. The external forces applied comprehend the weight of the roof transmitted to the pier (P_R) and the equivalent horizontal force (μP_R), i.e. the self-weight of the roof (γ_R) and the coefficient of friction (μ) are considered as aleatory variables. The lower, median and upper values of the aleatory variables ($X_{k,low}$, $X_{k,med}$ and $X_{k,up}$, respectively) are summarized in Table 2.

Table 2 – Characterization of the aleatory variables in terms of lower, median and upper values

X_k	$X_{k,low}$	$X_{k,med}$	$X_{k,up}$
$t_{parapet}$ [m]	0.10	0.13	0.15
t_{pier} [m]	0.35	0.38	0.40
γ_R [kN/m^2]	0.88	1.09	1.30
μ [-]	0.40	0.50	0.60

In the global model of the buildings, the street façade in the last floor is defined with 0.40 m of thickness. Considering that the thickness of the façade walls decreases along the height, approximately 0.05 m in each floor, the same variation is now assumed for the thickness of the central pier (t_{pier}). In addition, in the global model of the buildings, the parapet is defined with 0.15 m of thickness and 0.80 m of height. In this case, the thickness of the parapet ($t_{parapet}$) is considered between 0.10 m and 0.15 m.

The self-weight of the roof (γ_R) is defined by the interval of values proposed by (Ferreira and Farinha, 1974). In the global model of the buildings, this is defined equal to 1.30 kN/m^2. The dimensions *a* and *b*, defining the tributary area for the timber roof structure supported on the central pier (Figure 8 (a)), are assumed deterministic (a = 2.27 m and b = 3.90 m). The coefficient of friction (μ) between timber and masonry is defined from (Farinha and Reis, 1993; Zhang et al., 2008).
The aleatory variables are treated by a full factorial combination at two levels. For each of the Q=2^N models, the aleatory variables assume the values correspondent to the lower ($X_{k,low}$) and upper ($X_{k,up}$) values of the interval. Table 3 identifies the variables involved in the three out-of-plane mechanisms and the number of combinations/models considered for the analysis of the local seismic behaviour.

Table 3 – Combination of aleatory variables for each mechanism

Mech.	Variables X_k	N	Q=2^N
1	$t_{parapet}$, t_{pier}, γ_R, μ	4	16
2	$t_{parapet}$, t_{pier}, γ_R	3	8
3	$t_{parapet}$	1	2

6. Derivation of fragility functions

6.1. Global behaviour

Figure 11 shows the pushover curves obtained by performing non-linear static (pushover) analyses subjected to uniform (Unif) and triangular (Triang) load distributions in the direction parallel to the façade walls (X direction) and parallel to the side walls (Y direction), including negative (-) and positive (+) orientations. The pushover curves express the ratio between the base shear force and the weight of the structure (V/W) as a function of the average displacement of the roof weighted by the seismic modal mass of all nodes (*d*). The option for the average displacement represents a heuristic approach useful to define a curve representative of the whole structure in case of buildings with flexible diaphragms and/or in plan irregularities (Lagomarsino and Cattari, 2015). For more information on the global behaviour of the class of buildings check §4.1 from (Simões et al., 2019a).

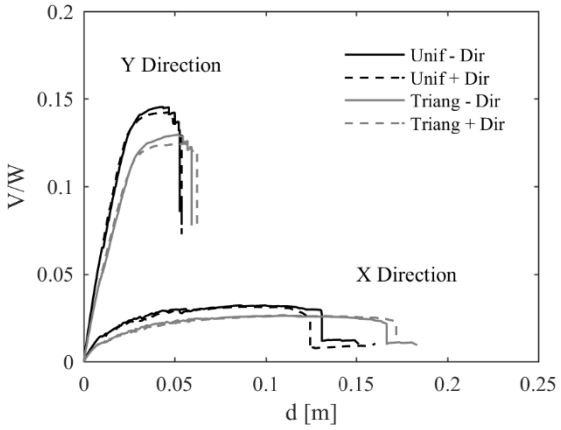

Figure 11 – Pushover curves: median values of the aleatory variables

Figure 12 presents the fragility curves parameters obtained from the all analyses performed, namely: (a) and (d) plot the median intensity measure IM_{LS} values that produces the attainment of the limit state threshold LS, in this case represented by the $PGA_{50\%}$ and performance levels (PLi, with i=1,…,4), (b) and (e) plot the dispersion in the capacity (β_C), and (c) and (f) plot dispersion in the seismic demand (β_D).
From Figure 12 (a) and (c) it is observed that there are small variations between the $PGA_{50\%}$ values obtained with the negative and positive directions (the coefficient of variation is lower than 5.7%) and between the uniform and triangular distributions (the coefficient of variation is lower than 10.4%) even though, the uniform distribution provides, in general, lower $PGA_{50\%}$ values. In what concerns the different performance levels, lower $PGA_{50\%}$ values are obtained for PL1 and PL2 in the X direction and for PL3 and PL4 in the Y direction.
Figure 12 (b) and (e) show a lower dispersion in the Y direction than in the X direction. The behaviour of the block of buildings in the Y direction is mainly governed by the response of the side solid walls, while the behaviour in the X direction is affected by the full set of aleatory variables considered. From Figure 12 (b), it emerges that the dispersion in the capacity (β_C) has the highest value for PL1 in the X direction. Although the macro-element scale is the criterion that defines, in general, the position of the DL in the pushover curves obtained for the X direction, as exemplified in Figure 13, it is also observed that for DL1 it is divided between the three criteria,

increasing therefore the dispersion in the capacity (β_C) for PL1. Moreover, the determination of DL1 is in general a difficult task because it is associated with a state of slight damage in the structure.

Finally, comparing the dispersion in the capacity (β_C) (Figure 12 (b) and (e)) and the dispersion in the seismic demand (β_D) (Figure 12 (c) and (f)), it is evident that the latter has higher contribution for the final value of dispersion $\beta_{G,PL}$ due to the large variability of possible ground-motion records.

Taking into account the small variations between the $PGA_{50\%}$ values obtained in the negative and positive directions and between the $PGA_{50\%}$ values obtained with the application of the uniform and triangular load distributions, it is proposed to set the minimum PGA value between these results, as this leads to the most demanding condition for the block of buildings. On the other hand, the dispersion in the seismic demand (β_D) is defined as the maximum value between the all results obtained (negative and positive directions with the uniform and triangular distributions). The dispersion related to the global seismic behaviour ($\beta_{G,PL}$) is defined according to Equation (6). Table 4 summarizes the parameters for the fragility curves associated with the global behaviour obtained in the X and Y directions.

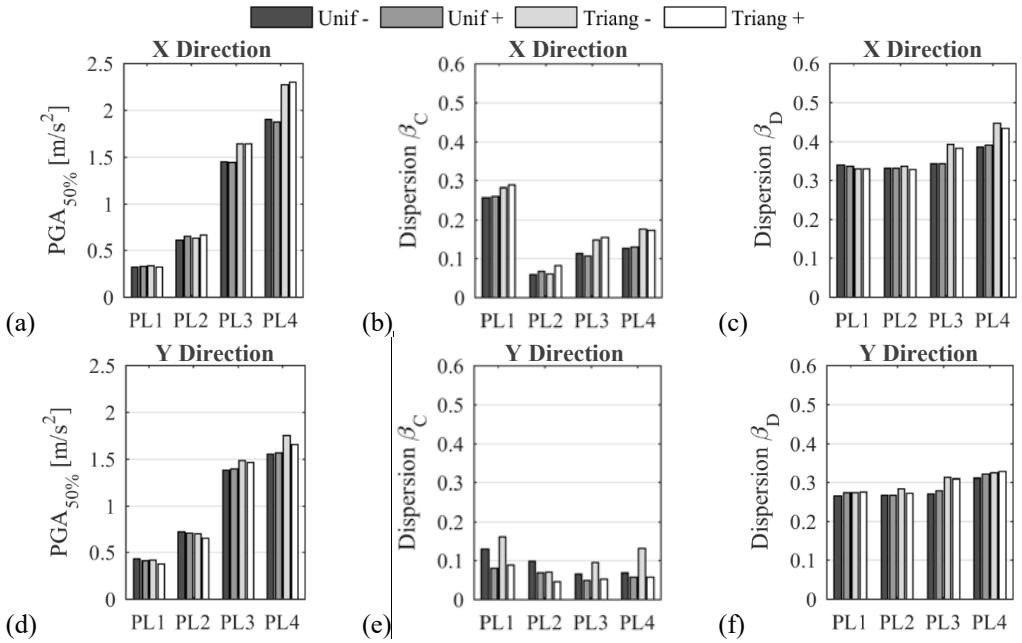

Figure 12 – Fragility curves parameters for the global behaviour: all analyses

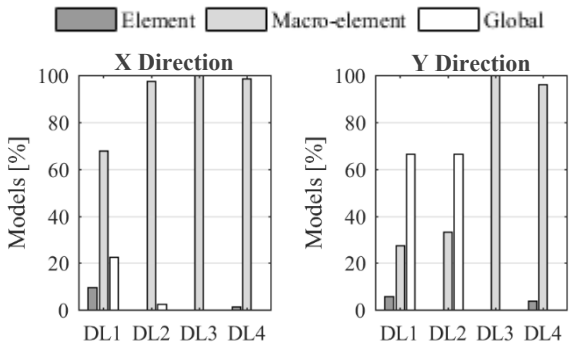

Figure 13 – Percentage of models as a function of the criteria for the definition of DL

Table 4 – Fragility curves parameters for the global behaviour: X and Y directions

PL	X Direction				Y Direction			
	$PGA_{50\%}$ [m/s^2]	β_C	β_D	$\beta_{G,PL}$	$PGA_{50\%}$ [m/s^2]	β_C	β_D	$\beta_{G,PL}$
1	0.303	0.260	0.340	0.428	0.379	0.087	0.275	0.289
2	0.608	0.068	0.336	0.343	0.650	0.048	0.284	0.288
3	1.434	0.107	0.394	0.408	1.371	0.061	0.314	0.320
4	1.855	0.125	0.446	0.464	1.544	0.064	0.329	0.336

It is proposed to derive the fragility curves associated with the global behaviour by considering the minimum between the fragility curves obtained in the X and Y directions, as this leads to the most demanding condition for the structure. Figure 14 shows the fragility curves obtained in the X and Y directions and the minimum combination between the two (represented by solid lines).
It is important to highlight that the resulting fragility curves are not a lognormal cumulative distribution function. The parameters that characterize the fragility curves are presented in Table 5. Here, the dispersion β_G is determined in an approximated way according to Equation **Erro! A origem da referência não foi encontrada.**, considering the values of PGA corresponding to the 84% and 16% percentile of the distribution.

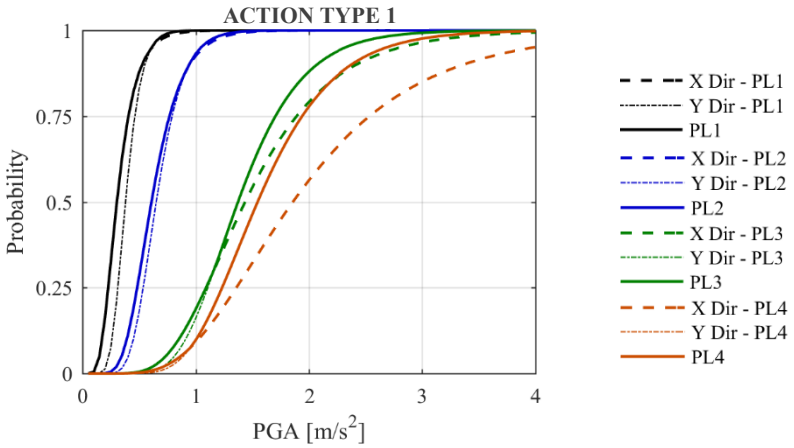

Figure 14 – Fragility curves for the global behaviour: combination between the fragility curves obtained in the X and Y directions

Table 5 – Fragility curves (approximated) parameters for the global behaviour

PL	$PGA_{50\%}$ [m/s^2]	$\beta_{G,PL}$
1	0.303	0.426
2	0.608	0.342
3	1.371	0.340
4	1.544	0.334

$$\beta_{G,PL} = \frac{1}{2}\left|\log(PGA_{84\%}) - \log(PGA_{16\%})\right| \quad (31)$$

6.2. Local behaviour

Figure 15 shows the capacity curves for the three mechanisms considered obtained by performing non-linear kinematic analyses. It is verified that the strength of Mech. 2 is higher than that of Mech. 1, but it is characterized by a lower displacement capacity. Mech. 3, which only involves the parapet, is the most critical mechanism as it exhibits the lowest strength and displacement capacity due to the reduced thickness of the element. In Mech. 1, the sudden decay of strength after 0.11 m displacement is consequence of the complete unthreading of the roof timber structure. For more information on the local behaviour of the class of buildings check §4.2 from (Simões et al., 2019a).

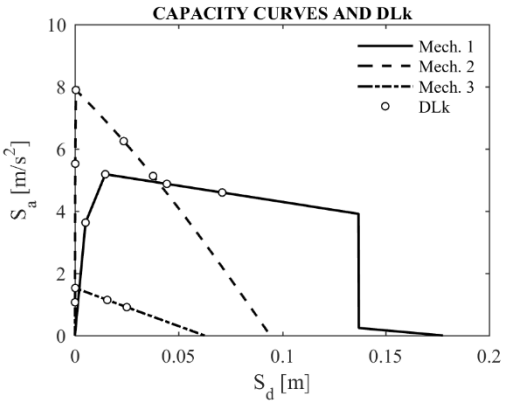

Figure 15 – Capacity curves for the local behaviour: median values of the aleatory variables

Figure 16 and Table 6 present the fragility curves parameters obtained for Mech. 1, Mech. 2 and Mech. 3. Figure 16 (a) plots the median intensity measure IM_{LS} values that produces the attainment of the limit state threshold LS, in this case represented by the $PGA_{50\%}$ and performance levels (PLi). Here, only the results concerning the attainment of PL1 and PL2 are presented provided that PL3 and PL4 are coincident with PL2 (i.e. the PGA values compatible with PL2, PL3 and PL4 are the same). This is justified because the attainment of PL2 corresponds to the final equilibrium condition of the mechanisms. In this case, Mech. 3 is the most vulnerable case, followed by Mech. 1 and Mech. 2.

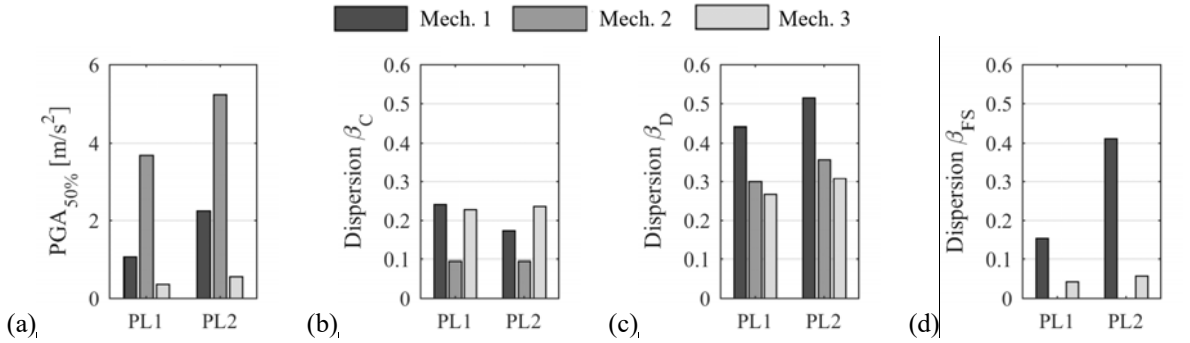

Figure 16 – Fragility curves parameters for the local behaviour

Table 6 – Fragility curves parameters for the local behaviour

Mech.	PL	$PGA_{50\%}$ [m/s^2]	β_C	β_D	β_{FS}	β_{PL}
1	1	1.063	0.241	0.441	0.154	0.526
	2	2.248	0.173	0.514	0.412	0.681
2	1	3.683	0.095	0.301	0	0.315
	2	5.231	0.096	0.358	0	0.370
3	1	0.356	0.229	0.267	0.042	0.354
	2	0.558	0.236	0.309	0.058	0.393

Figure 16 (b) provides the corresponding dispersion in the capacity (β_C) for Mech. 1, Mech. 2 and Mech. 3, where it is observed that Mech. 2 presents the lowest dispersion from all. Figure 16 (c) presents the dispersion in the seismic demand (β_D). These results are in general higher than the ones obtained with the analysis of the global seismic behaviour for PL1 and PL2 because they also take into account the filtering effect of the building.

In fact, an additional contribution to the dispersion needs to be considered in the analysis of the local behaviour. This additional contribution is referred here as the dispersion in the floor response spectrum (β_{FS}) and takes into account the aleatory uncertainties in the determination of the dynamic characteristics of the main structure that influence the filtering effect and the determination of the floor response spectrum. This dispersion is also estimated according to Equation (6). The $PGA_{84\%}$ and $PGA_{16\%}$ values that produces the attainment of PL are determined by considering each mechanism, defined by the median properties of the aleatory variables, and by applying the iterative procedure to define the floor response spectrum, as referred in §4.4. However, in this case, the period of the main structure ($T_{k,PLk}$) and the PGA value compatible with PL at the global scale ($PGA_{PL,G}$), are defined as the values corresponding to the 84% and 16% percentiles of the building models defined by the aleatory variables.

Figure 16 (d) plots the dispersion in the floor response spectrum (β_{FS}) showing that: 1) in case of Mech. 1, the dispersion for PL2 is higher than the dispersion for PL1 because to activate the mechanism a higher value of PGA is necessary (Figure 16 (a)), and 2) in case of Mech. 2 and Mech. 3 the dispersion is close to zero, because the computation of the PGA is almost not affected by the filtering effect of the building.

Taking this additional contribution, the dispersion related to the local seismic behaviour ($\beta_{L,PL}$), presented in Table 6, is defined according to:

$$\beta_{L,PL} = \sqrt{\beta_C^2 + \beta_D^2 + \beta_{FS}^2} \tag{32}$$

In reference to §5.3.1, two possible scenarios were identified for the local seismic behaviour of the buildings related to: 1) the last floor of the building and 2) the parapet. These were assumed as epistemic uncertainties and treated by the logic-tree approach. It is now proposed to determine the $PGA_{50\%}$ and the dispersion (β_{PL}) associated with each scenario taking into account the probability/reliability attributed to the different options. For the first scenario, the parameters are determined according to Equation (33) and Equation (34):

$$PGA_{50\%,LastFloor} = 0.70 PGA_{50\%,Mech1} + 0.30 PGA_{50\%,Mech2} \tag{33}$$

$$\beta_{LastFloor} = \sqrt{0.70\beta_{L,Mech1}^2 + 0.30\beta_{L,Mech2}^2} \quad (34)$$

As referred for the analysis of the global seismic behaviour (§6.1), the previous equations are an approximation, as the fragility curves obtained from the combination of the two possible scenarios are not a lognormal cumulative distribution function.

For the second scenario, the "no problem" hypothesis (see Figure 10) is characterized by a PGA that tends to infinity. Thus, the parameters that define the fragility curves associated with this scenario are obtained directly from the ones determined for Mech. 3 (Table 6), but imposing that the probability cannot exceed 0.60, which corresponds to the reliability/weight of this hypothesis (Figure 10 (b)).

The parameters that characterize the fragility curves associated with the local behaviour are presented in Table 7. Figure 17 provides the resulting fragility curves for both scenarios.

Table 7 – Fragility curves (approximated) parameters for the local behaviour

Scenario	PL	$PGA_{50\%}$ [m/s^2]	$\beta_{L,PL}$
Last Floor	1	1.865	0.464
	2	3.116	0.611
Parapet	1	0.363	0.334
	2	0.562	0.391

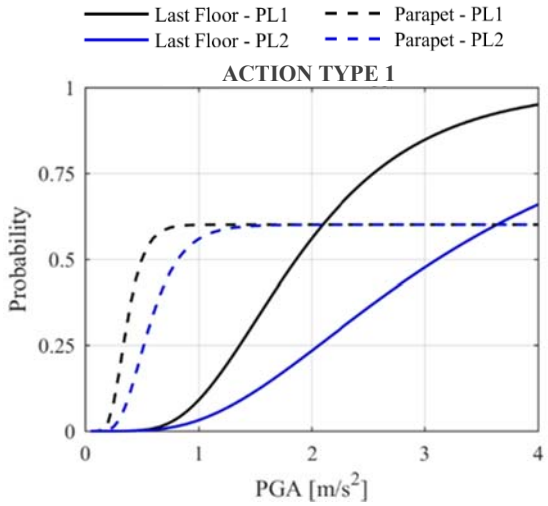

Figure 17 – Fragility curves for the local behaviour (note that the upper limit for the parapet collapse has a probability of 60%, as discussed in §5.3.1)

6.3. Combination between global and local behaviour

In order to derive the final fragility curves, it is first necessary to combine the global and the local seismic behaviour in the Y direction and after to combine the results in the X and Y directions.

The contribution of the local behaviour is limited to the mechanisms involving the last floor of the buildings (first scenario). Notwithstanding the relevance of the second scenario for the life safety, the simple overturning of the parapets is secondary for the verification of the main structure at a global scale. In addition, it is assumed that PL1 at the local scale is not relevant at a global scale. On the other hand, the occurrence of PL2 at the local scale is related both to the activation of the mechanism and to the out-of-plane collapse (i.e. the PGA values compatible with PL2, PL3 and PL4 are the same). Thus, it is proposed to add the contribution of PLk greater than PL1 at the local scale to the corresponding PLk at the global scale. In what concerns the contribution of the global behaviour, the different performance limit states are directly correlated to the behaviour of the main structure in the Y direction. The resulting fragility curves are defined by:

$$P_{PLk} = P_{G,PLk} + (1 - P_{G,PLk})P_{L,PLk} \quad (35)$$

Finally, it is proposed to consider the minimum between the results obtained in the X and Y directions, the later including the local behaviour, as this leads to the most demanding condition for the group of buildings. Figure 18 shows the fragility curves in the X and Y directions and the minimum combination between the two (represented by solid lines). These define the final fragility curves for the class of buildings. The parameters that characterize the fragility curves are given in Table 8, determined in an approximated way according to Equation **Erro! A origem da referência não foi encontrada.**.

The discrete probability associated with the different damage states is determined following the procedure presented in §2. The code seismic action for Lisbon: type 1 (PGA*S = 1.94 m/s^2 with a return period of 475 years)

is considered for the estimation of the damage distribution. Figure 19 shows the corresponding probability damage distribution. The values obtained considering only the global behaviour are also included for comparison. The mean and variation parameters are not very different in the case of global and combined behaviour. This is not a general result and it depends on the relative position between the two basic fragility curves (see Table 5 and 7). Indeed, in particular the global response is significantly affected by the seismic action type. To clarify this issue, Figure 20 and Figure 21 illustrate the effect of the combination varying the seismic action type considered (see Simões et al. (2019a) for more details on results associated to the seismic type 2). It is observed that the local behaviour has in both cases a negligible contribution for the definition of PL1 and PL2, but an important contribution for the other PLk in particular in case of the seismic type 2.

The results put in evidence the high seismic vulnerability of the buildings. It is estimated that there is about 50% probability of having very heavy damage (DS4) and about 30% probability of collapse (DS5). As expected, the contribution of the local seismic behaviour increases the final vulnerability. Moreover, according to Figure 17, collapse of the parapets for seismic action type I in Lisbon (PGA*S=1.94 m/s^2) is guaranteed. Here, it is important to refer that these results represent the upper line of the expected distribution of damage, taking into account that: 1) the worst case scenario was considered in the main steps of the methodology and, 2) the recommendation given by the Portuguese National Annex to the EC8-3 (IPQ, 2017) to reduce of the reference peak ground acceleration for the assessment of existing buildings was disregarded.

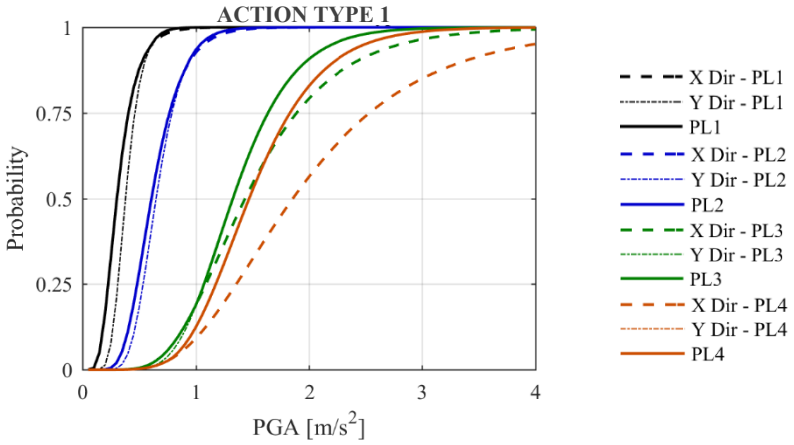

Figure 18 – Final fragility curves: combination between X and Y directions, the latter including the local behaviour

Table 8 – Final fragility curves (approximated) parameters

PL	$PGA_{50\%}$ [m/s^2]	β_{PL}
1	0.303	0.426
2	0.608	0.341
3	1.326	0.318
4	1.470	0.326

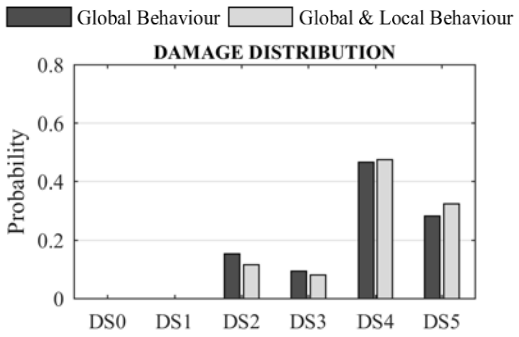

Damage distribution		DS0	DS1	DS2	DS3	DS4	DS5
Action Type 1 PGA*S = 1.94 m/s^2	Global Behaviour	0.000	0.000	0.154	0.094	0.467	0.285
	Global & Local Behaviour	0.000	0.000	0.116	0.082	0.475	0.327

Figure 19 – Distribution of damage for seismic action type 1 (PGA*S=1.94 m/s^2)

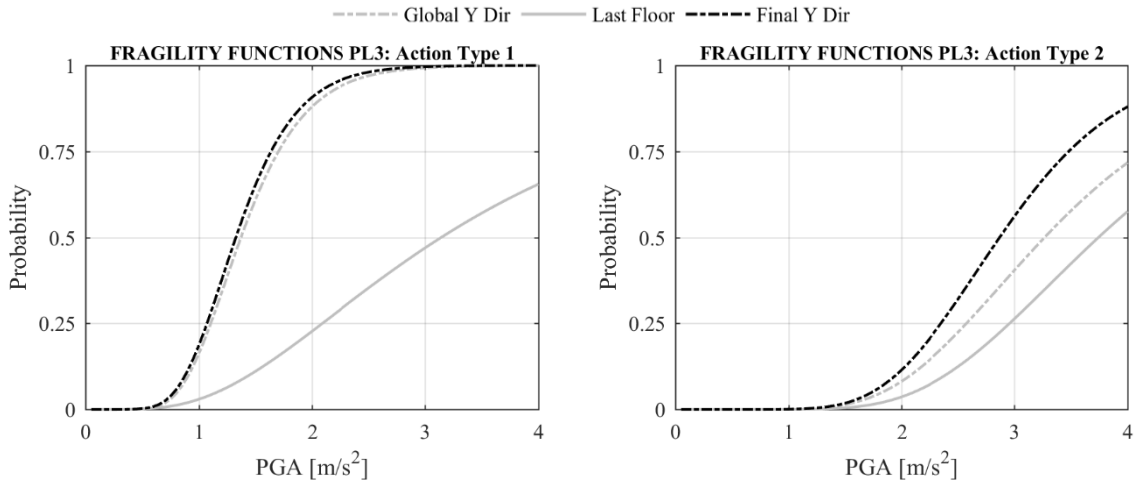

Figure 20 – Combination of the fragility functions in the Y direction for PL3: seismic action type 1 (left) and type 2 (right)

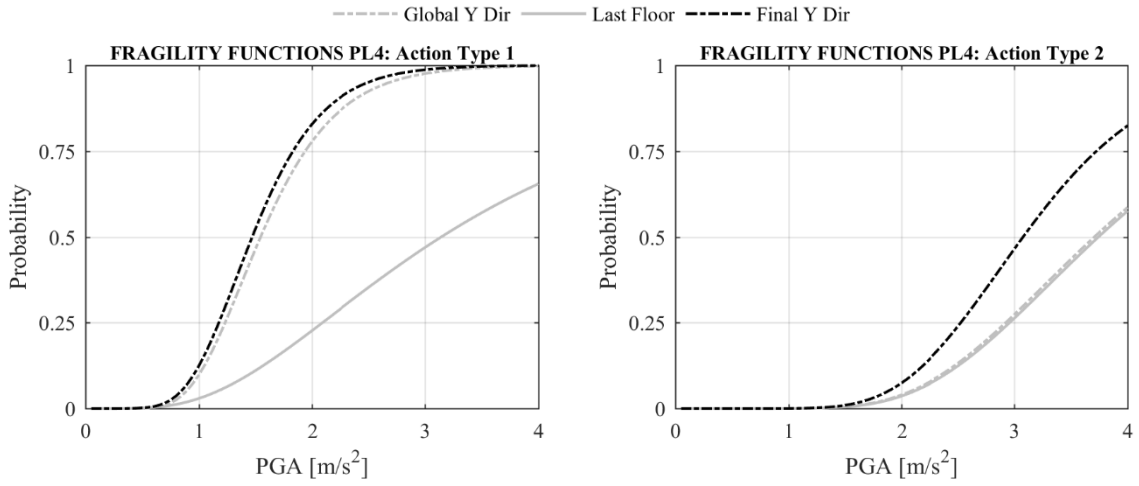

Figure 21 – Combination of the fragility functions in the Y direction for PL4: seismic action type 1 (left) and type 2 (right)

7. Final Remarks

The article presents a procedure for the derivation of fragility functions for unreinforced masonry building classes. The approach adopted comprehends the generation of fragility functions for the in-plane and out-of-plane response following different criteria and methods of analyses. The individual fragility curves are after combined in order to define a single fragility curve representative of the class of buildings.
The contributions for the dispersion of the fragility functions account for:

- The variability in the definition of the capacity, evaluated by the Monte Carlo Method for the analysis of the global behaviour and the Response Surface Technique for the local behaviour. Notwithstanding the lower computational burden, the application of the Response Surface Method for the global behaviour would not be feasible for the comprehensive evaluation of the uncertainty propagation taking into account the complexity of the analysis and the higher number of aleatory variables considered.
- The aleatory uncertainty in the definition of the seismic demand, evaluated starting from a selection of a set of real ground-motion records compatible with the geophysical characteristics of the reference code seismic action.

- The aleatory uncertainty in the definition of the modified/floor response spectrum, when the local mechanisms are located in the upper level of the building, in order to account the variability of the dynamic filtering effect provided by the main structure.

The procedure is applied to a class of URM tall buildings, constructed between the 19th and 20th centuries in Lisbon, Portugal. The results put in evidence their high seismic vulnerability and the urgent need for structural retrofitting in order to reduce potential losses due to future earthquakes. The companion article (Simões et al., 2019a) deals with the derivation of the fragility functions for different classes of buildings. This aims to evaluate the fragility curves representative of the class of buildings at the territory level. The fragility curves obtained for this type of URM buildings are compared with the fragility curves derived in previous studies in Simões et al. (2019b). The final objective of this work is to perform the overall seismic evaluation of the buildings constructed in Lisbon in this period, which are assumed the most vulnerable of the building typologies in Lisbon.

Acknowledgements: The first author would like to acknowledge the financial support of *Fundação para a Ciência e a Tecnologia* (FCT, *Ministério da Educação e Ciência*, Portugal) through the scholarship PD/BD/106076/2015 through the FCT Doctoral Program: Analysis and Mitigation of Risks in Infrastructures, INFRARISK- (http://infrarisk.tecnico.ulisboa.pt).

References

Appleton JG (2005) Reabilitação de Edifícios "Gaioleiros. 1st ed. Lisboa: Edições Orion (In Portuguese).

Beyer K, Mangalathu S. (2004) Numerical Study on the Peak Strength of Masonry Spandrels with Arches. Journal of Earthquake Engineering 2014; 18: 169–186. DOI: 10.1080/13632469.2013.851047.

Bracchi S, Rota M, Magenes G, Penna A. (2016) Seismic assessment of masonry buildings accounting for limited knowledge on materials by Bayesian updating. Bulletin of Earthquake Engineering 2016; 14(8): 2273–2297. DOI: 10.1007/s10518-016-9905-8.

Calderini C, Cattari S, Lagomarsino S. (2009) In-plane strength of unreinforced masonry piers. Earthquake Engineering and Structural Dynamics 2009; 38: 243–267. DOI: 10.1002/eqe.

Candeias P. (2008) Avaliação da vulnerabilidade sísmica de edifícios de alvenaria. PhD Thesis. Universidade do Minho. Guimarães (In Portuguese).

Cattari S, Lagomarsino S, Marino S. (2015) Reliability of nonlinear static analysis in case of irregular urm buildings with flexible diaphragms. SECED 2015 Conference: Earthquake Risk and Engineering towards a Resilient World, Cambridge, UK: 2015.

Cattari S, Lagomarsino S. (2008) A strength criterion for the flexural behaviour of spandrels in un-reinforced masonry walls. Proceedings of the 14th Earthquake Conference on Earthquake Engineering, Beijing: 2008.

Cattari S, Lagomarsino S. (2013a) Masonry Structures. In: Sullivan T, Calvi GM, editors. Developments in the field of displacement based seismic assessment. IUSS Press, 2013. DOI: 10.1002/ejoc.201200111.

Cattari S, Lagomarsino S. (2013b) Seismic assessment of mixed masonry-reinforced concrete buildings by non-linear static analyses. Earthquake and Structures 2013; 4(3): 241–264. DOI: 10.12989/eas.2013.4.3.241.

CEN (2004) Eurocode 8: Design of structures for earthquake resistance. Part 1: General rules, seismic actions and rules for buildings Eurocode, EN 1998-1. European Committee for Standardization (CEN), Brussels: 2004.

D'Ayala D, Paganoni S. (2011) Assessment and analysis of damage in L'Aquila historic city centre after 6th April 2009. Bulletin of Earthquake Engineering 2011; 9(1): 81–104. DOI: 10.1007/s10518-010-9224-4.

Degli Abbati S, Cattari S, Lagomarsino S. (2018) Theoretically-based and practice-oriented formulations for the floor spectra evaluation. Earthquake and Structures 2018: (In Press).

Degli Abbati S, Cattari S, Marassi I, Lagomarsino S. (2014) Seismic Out-of-Plane Assessment of Podestà Palace in Mantua (Italy). Key Engineering Materials 2014; 624: 88–96. DOI: 10.4028/www.scientific.net/KEM.624.88.

Degli Abbati S, Lagomarsino S. (2017) Out-of-plane static and dynamic response of masonry panels. Engineering Structures 2017; 150: 803–820. DOI: 10.1016/j.engstruct.2017.07.070.

Degli Abbati S. (2016) Seismic Assessment of Single-Block Rocking Elements in Masonry Structures. PhD Thesis. Università Degli Studi de Genova. Genova.

Doherty K, Griffith MC, Lam N, Wilson J. (2002) Displacement-based seismic analysis for out-of-plane bending

of unreinforced masonry walls. Earthquake Engineering and Structural Dynamics 2002; 31(4): 833–850. DOI: 10.1002/eqe.126.

Douglas J, Seyedi D M, Ulrich T, Modaressi H, Foerster E, Pitilakis K, Pitilakis D, Karatzetzou A, Gazetas G, Garini E, Loli M. (2015) Evaluation of seismic hazard for the assessment of historical elements at risk: description of input and selection of intensity measures. Bulletin of Earthquake Engineering 13(1): 49–65. DOI: 10.1007/s10518-014-9606-0.

Endo Y, Pelà L, Roca P. (2017) Review of Different Pushover Analysis Methods Applied to Masonry Buildings and Comparison with Nonlinear Dynamic Analysis. Journal of Earthquake Engineering 2017; 21(8): 1234–1255. DOI: 10.1080/13632469.2016.1210055.

Erberik MA. (2008) Generation of fragility curves for Turkish masonry buildings considering in-plane failure modes. Earthquake Engineering & Structural Dynamics 2008; 37(3): 387–405. DOI: 10.1002/eqe.760.

Fajfar P. (2000) A Nonlinear Analysis Method for Performance-Based Seismic Design. Earthquake Engineering and Structural Dynamics 2000; 16(3): 573–592. DOI: 10.1193/1.1586128.

Farinha J, Reis A. (1993) Tabelas Técnicas. 2nd ed. Setúbal: Edição P.O.B. (In Portuguese).

Ferreira V, Farinha J. (1974) Tabelas Técnicas para Engenharia Civil. 7th ed. Lisboa: Técnica. Associação de Estudantes do Instituto Superior Técnico (In Portuguese).

Franchin P, Pagnoni T. (2018) A General Model of Resistance Partial Factors for Seismic Assessment and Retrofit. 16th European Conference on Earthquake Engineering, Thessaloniki.

Giongo I, Dizhur D, Tomasi R, Ingham JM. (2013) In-plane assessment of existing timber diaphragms in URM buildings via quasi-static and dynamic in situ tests. Advanced Materials Research 2013; 778: 495–502. DOI: 10.4028/www.scientific.net/AMR.778.495.

Griffith MC, Lam NTK, Wilson JL, Doherty K. (2004) Experimental investigation of unreinforced brick masonry walls in flexure. Journal of Structural Engineering 2004; 130(3): 423–432. DOI: 10.1061/(ASCE)0733-9445(2004)130:3(423).

Grünthal G. (1998) European Macroseismic Scale 1998: EMS-98. Chaiers Du Centre Européen de Géodynamique et de Séismologie. Luzembourg.

Haddad J, Cattari S, Lagomarsino S. (2017) The use of sensitivity analysis for the probabilistic-based seismic assessment of existing buildings. 16th World Conference on Earthquake Engineering, Santiago Chile.

Housner GW. (1963) The behavior of inverted pendulum structures during earthquakes. Bulletin of the Seismological Society of America 1963; 53(2): 403–417.

IPQ (2010) Eurocódigo 8 - Projecto de estruturas para resistência aos sismos. Parte 1: Regras gerais, acções sísmicas e regras para edifícios, NP EN 1998-1:2010. Instituto Português Da Qualidade (IPQ). Caparica (In Portuguese).

IPQ (2017) Eurocódigo 8 – Projeto de estruturas para resistência aos sismos Parte 3: Avaliação e reabilitação de edifícios, NP EN 1998-3:2017. Instituto Português Da Qualidade (IPQ). Caparica (In Portuguese).

JCSS, Joint Committee on Structural Safety (2011) Probabilistic Model Code. Part 3: Resistance Models. 3.2. Masonry Properties.

Kržan M, Gostič S, Cattari S, Bosiljkov V. (2015) Acquiring reference parameters of masonry for the structural performance analysis of historical buildings. Bulletin of Earthquake Engineering 2015; 13(1): 203–236. DOI: 10.1007/s10518-014-9686-x.

Lagomarsino S, Cattari S. (2014) Fragility functions of masonry buildings. In: Pitilakis K, Crowley H, Kaynia A, editors. SYNER-G: Typology Definition and Fragility Functions for Physical Elements at Seismic Risk, Buildings, Lifelines, Transportation Networks and Critical Facilities, Geotechnical, Geological and Earthquake Engineering, 27, Springer; 2014. DOI: 10.1007/978-94-007-7872-6_5.

Lagomarsino S, Cattari S. (2015) Seismic Performance of Historical Masonry Structures Through Pushover and Nonlinear Dynamic Analyses. In: Ansal A, editor. Perspectives on European Earthquake Engineering and Seismology, Geotechnical, Geological and Earthquake Engineering, 39, vol. 39, Springer International Publishing; 2015. DOI: 10.1007/978-3-319-16964-4.

Lagomarsino S, Penna A, Galasco A, Cattari (2013) S. TREMURI program: An equivalent frame model for the nonlinear seismic analysis of masonry buildings. Engineering Structures 2013; 56: 1787–1799. DOI:

10.1016/j.engstruct.2013.08.002.

Lagomarsino S, Penna A, Galasco A, Cattari S. (2012) TREMURI program: seismic analyses of 3D masonry buildings.

Lagomarsino S. (2015) Seismic assessment of rocking masonry structures. Bulletin of Earthquake Engineering 2015; 13(1): 97–128. DOI: 10.1007/s10518-014-9609-x.

Liel AB, Haselton CB, Deierlein GG, Baker JW. (2009) Incorporating modelling uncertainties in the assessment of seismic collapse risk of buildings. Structural Safety 2009; 31: 197–211. DOI: 10.1016/j.strusafe.2008.06.002.

Lourenço PB, Mendes N, Ramos LF, Oliveira D V. (2011) Analysis of Masonry Structures Without Box Behavior. International Journal of Architectural Heritage 2011; 5: 369–382. DOI: 10.1080/15583058.2010.528824.

Macedo L, Castro JM. (2017) SelEQ: An advanced ground motion record selection and scaling framework. Advances in Engineering Software 2017; 114: 32–47. DOI: 10.1016/j.advengsoft.2017.05.005.

Marino S, Cattari S, Lagomarsino S. (2018) Use of nonlinear static procedures for irregular URM buildings in literature and codes. 16th European Conference on Earthquake Engineering, Thessaloniki.

Mendes N, Lourenço PB, Campos-Costa A. (2014) Shaking table testing of an existing masonry building: assessment and improvement of the seismic performance. Earthquake Engineering & Structural Dynamics 2014; 43(2): 247–266. DOI: 10.1002/eqe.2342.

MIT (2009) Istruzioni per l'applicazione delle "Norme tecniche per le costruzioni" di cui al Decreto Ministeriale 14/01/2008. Ministero Delle Infrastrutture e Dei Trasporti (MIT). Roma (In Italian).

NTC (2008) Norme tecniche per le costruzioni (NTC). Decreto Ministeriale 14/01/2008. Roma (In Italian).

NZSEE (2017) The Seismic Assessment of Existing Buildings. Technical Guidelines for Engineering Assessments. Part C - Detailed Seismic Assessment. Part C8 - Unreinforced Masonry Buildings. New Zealand Society for Earthquake Engineering (NZSEE) Inc. Wellington.

Ottonelli D, Cattari S, Lagomarsino S. (2015) Urban risk assessment: fragility functions for masonry buildings. In: Rudas IJ, editor. Recent Advances in Mechanics, Mechatronics and Civil, Chemical and Industrial Engineering. Mathematics and Computers in Science and Engineering Series, 49.

Penna A, Morandi P, Rota M, Manzini CF, da Porto F, Magenes G. (2014) Performance of masonry buildings during the Emilia 2012 earthquake. Bulletin of Earthquake Engineering 2014; 12(5): 2255–2273. DOI: 10.1007/s10518-013-9496-6.

Pitilakis K, Crowley H, Kaynia AM. (2014) SYNER-G: Typology Definition and Fragility Functions for Physical Elements at Seismic Risk. Springer; 2014. DOI: 10.1007/978-94-007-7872-6.

Porter K, Kennedy R, Bachman R. (2007) Creating fragility functions for performance-based earthquake engineering. Earthquake Spectra 2007; 23(2): 471–489. DOI: 10.1193/1.2720892.

Rebelo A, Guedes JM, Quelhas B, Ilharco T. (2015) Assessment of the mechanical behaviour of tabique walls through experimental tests. Proceedings of the 2nd International Conference on Historic Earthquake-Resistant Timber Frames in the Mediterranean Region, Lisboa.

Rota M, Penna A, Magenes G. (2010) A methodology for deriving analytical fragility curves for masonry buildings based on stochastic nonlinear analyses. Engineering Structures 2010; 32(5): 1312–1323. DOI: 10.1016/j.engstruct.2010.01.009.

RSEU (1903) Regulamento de Salubridade das Edificações Urbanas (RSEU), Decreto de 14/02/1903 (In Portuguese).

Rubinstein RY. (2011) Simulation and the Monte Carlo Method. John Wiley & Sons, Inc.

Silva V, Crowley H, Varum H, Pinho R. (2015) Seismic risk assessment for mainland Portugal. Bulletin of Earthquake Engineering 2015; 13: 429–457. DOI: 10.1007/s10518-014-9630-0.

Simões A, Appleton JG, Bento R, Caldas J V, Lourenço PB, Lagomarsino S. (2017) Architectural and Structural Characteristics of Masonry Buildings between the 19th and 20th Centuries in Lisbon, Portugal. International Journal of Architectural Heritage 2017; 11(4): 457–474. DOI: 10.1080/15583058.2016.1246624.

Simões A, Bento R, Cattari S, Lagomarsino S. (2014) Seismic performance-based assessment of "Gaioleiro" buildings. Engineering Structures 2014; 80: 486–500. DOI: 10.1016/j.engstruct.2014.09.025.

Simões A, Bento R, Lagomarsino S, Lourenço PB. (2016) Simplified evaluation of seismic vulnerability of early

20th century masonry buildings in Lisbon. Proceedings of the 10th International Conference on Structural Analysis of Historical Constructions, Leuven: 2016.

Simões A, Milošević J, Meireles H, Bento R, Cattari S, Lagomarsino S. (2015) Fragility curves for old masonry building types in Lisbon. Bulletin of Earthquake Engineering 2015; 13(10): 3083–3105. DOI: 10.1007/s10518-015-9750-1.

Simões A. (2018) Evaluation of the seismic vulnerability of the unreinforced masonry buildings constructed in the transition between the 19th and 20th centuries in Lisbon, Portugal. PhD Thesis. Instituto Superior Técnico, Universidade de Lisboa. Lisboa.

Simões AG, Bento R, Lagomarsino S, Cattari S, Lourenço PB. (2019a) Fragility functions for tall URM buildings around early 20th century in Lisbon. Part 2: application to different classes of buildings. International Journal of Architectural Heritage (in revision).

Simões AG, Bento R, Lagomarsino S, Cattari S, Lourenço PB. (2019b) Seismic assessment of nineteenth and twentieth centuries URM buildings in Lisbon: structural features and derivation of fragility curves. Bulletin of Earthquake Engineering, Springer. DOI: 10.1007/s10518-019-00618-z.

Simões AG, Bento R, Lagomarsino S, Lourenço PB. (2018) The seismic assessment of masonry buildings between the 19th and 20th centuries in Lisbon - Evaluation of uncertainties. Proceedings of the 10th International Masonry Conference, Milan: 2018.

Turnšek V, Čačovič F. (1970) Some experimental results on the strength of brick masonry walls. Proceedings of the 2nd International Brick Masonry Conference, Stoke-on-Trent.

Turnšek V, Sheppard P. (1980) The shear and flexural resistance of masonry walls. Proceedings of the International Research Conference on Earthquake Engineering, Skopje.

Vanin F, Zaganelli D, Penna A, Beyer K. (2017) Estimates for the stiffness, strength and drift capacity of stone masonry walls based on 123 quasi-static cyclic tests reported in the literature. Bulletin of Earthquake Engineering 2017: 1–45. DOI: 10.1007/s10518-017-0188-5.

Zhang P, Nagae T, McCormick J, Ikenaga M, Katsuo M, Nakashima M. (2008) Friction-based sliding between steel and steel, steel and concrete, and wood and stone. Proceedings of the 14th World Conference on Earthquake Engineering.